Journal of proteome research

pubs.acs.org/jpr

Article

Optimal Dissociation Methods Differ for *N*- and *O*-Glycopeptides

Nicholas M. Riley, Stacy A. Malaker, Marc D. Driessen, and Carolyn R. Bertozzi*

Cite This: *J. Proteome Res.* 2020, 19, 3286−3301

Read Online

ACCESS | Metrics & More | Article Recommendations | Supporting Information

ABSTRACT: Site-specific characterization of glycosylation requires intact glycopeptide analysis, and recent efforts have focused on how to best interrogate glycopeptides using tandem mass spectrometry (MS/MS). Beam-type collisional activation, i.e., higher-energy collisional dissociation (HCD), has been a valuable approach, but stepped collision energy HCD (sceHCD) and electron transfer dissociation with HCD supplemental activation (EThcD) have emerged as potentially more suitable alternatives. Both sceHCD and EThcD have been used with success in large-scale glycoproteomic experiments, but they each incur some degree of compromise. Most progress has occurred in the area of *N*-glycoproteomics. There is growing interest in extending this progress to *O*-glycoproteomics, which necessitates comparisons of method performance for the two classes of glycopeptides. Here, we systematically explore the advantages and disadvantages of conventional HCD, sceHCD, ETD, and EThcD for intact glycopeptide analysis and determine their suitability for both *N*- and *O*-glycoproteomic applications. For *N*-glycopeptides, HCD and sceHCD generate similar numbers of identifications, although sceHCD generally provides higher quality spectra. Both significantly outperform EThcD methods in terms of identifications, indicating that ETD-based methods are not required for routine *N*-glycoproteomics even if they can generate higher quality spectra. Conversely, ETD-based methods, especially EThcD, are indispensable for site-specific analyses of *O*-glycopeptides. Our data show that *O*-glycopeptides cannot be robustly characterized with HCD-centric methods that are sufficient for *N*-glycopeptides, and glycoproteomic methods aiming to characterize *O*-glycopeptides must be constructed accordingly.

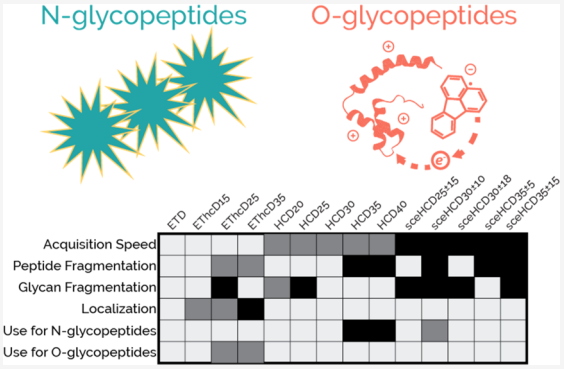

KEYWORDS: *glycoproteomics, N-glycopeptides, O-glycopeptides, tandem MS, fragmentation, electron transfer dissociation, stepped collision energy high-energy collisional dissociation, ETD, EThcD, sceHCD*

INTRODUCTION

Protein glycosylation is a complex post-translational modification that governs a diverse range of biological functions, serving as a biophysical and biochemical interface at the cell surface.[1] Glycosylation can be grouped into two main classes, *N*- and *O*-linked, where glycans are attached at asparagine or serine/threonine residues, respectively. The pool of glycans that decorate proteins is heterogeneous, which leads to extensive microheterogeneity across glycosites; moreover, *N*-glycosites fundamentally differ from *O*-glycosites in both the glycans that modify them and the regions of proteins where they generally occur.[2] Thus, intact glycopeptide characterization, which provides the opportunity to probe microheterogeneity by localizing glycan modifications to specific residues, is an imperative, yet challenging component to modern glycoproteomic analysis. Tandem mass spectrometry (MS/MS) serves as the center piece in these efforts, but the path to glycopeptide identification is not one-dimensional. Numerous approaches comprise the glycoproteomics toolkit, and efforts to improve our analytical methods are ongoing.[3−9]

Beam-type collisional activation, termed higher-energy collisional dissociation (HCD) on Orbitrap systems,[10] and electron transfer dissociation (ETD) are two of the more widely used MS/MS dissociation methods for glycopeptide characterization.[10−15] They are complementary to each other; ETD generates mostly c/z·-type peptide backbone fragments that retain intact glycan moieties with few glycan dissociation events, while HCD fragments glycans and also produces b/y-type peptide backbone fragments that tend to lose all or part of their glycan modifications during the activation process.[16−20] Many approaches pair the two dissociation methods within the same analysis to capitalize on their complementary nature.[21−29] In fact, HCD followed by product-dependent ETD (HCD-pd-ETD) has become arguably the most common glycoproteomic method to incorporate ETD. Here, glycopeptide-specific oxonium ions derived from glycan fragmentation in "scout

Received: April 2, 2020
Published: June 5, 2020

HCD" scans are used to trigger subsequent ETD fragmentation of the putative glycopeptide precursor.[30−32]

One challenge of ETD-based fragmentation is poor dissociation efficiency, especially for low-charge-density precursors like glycopeptides.[15] To address this issue, hybrid methods that use vibrational activation to provide supplemental energy for ETD reactions have emerged and gained traction in glycoproteomics, with the most popular being ETD followed by supplemental HCD (EThcD).[33−45] Even so, HCD remains widely used in *N*-glycoproteomics.[46−57] Tryptic *N*-glycopeptides tend to harbor only one potential glycosite, as defined by its sequon N-X-S/T, where X represents any amino acid other than proline, which limits dependence on peptide fragments that retain intact glycans. HCD of *N*-glycopeptides also often generates b/y-type fragments that retain an *N*-acetylglucosamine (GlcNAc) moiety, which provide clues to glycosite localization. Conversely, *O*-glycopeptides generally have multiple serine and/or threonine residues that serve as potential glycosites, so *O*-glycoproteomic methods largely utilize ETD and EThcD to localize modified residues using c/z·-type fragments that retain the intact glycan.[58−74]

Recently, several groups have observed that higher HCD collision energies tend to provide better peptide backbone fragmentation, while lower collision energies are often advantageous for glycan fragmentation and, as such, have opted for stepped collision energy HCD (sceHCD) methods.[75−77] In the sceHCD regime, total precursor ion accumulation time per scan is divided into multiple (usually three) equal parts, and ions accumulated in each separate event are fragmented at different HCD collision energies. Product ions from each dissociation step are collected in the same reaction cell prior to mass analysis and are then analyzed together in one MS/MS scan. In 2017, Liu et al. used sceHCD methods for the identification of ∼10,000 *N*-glycosites from five mouse tissues,[78] which contributed to its popularity in recent *N*-glycopeptide analysis.[79−86] A few studies have looked to extend the application of sceHCD to *O*-glycopeptides,[75,76,79,87,88] but this has not been as widespread. Limited comparisons between sceHCD and ETD methods have been performed for *N*-glycopeptides,[78] as have comparisons of HCD and EThcD for *O*-glycopeptides;[64,69] however, a comprehensive head-to-head comparison of standard HCD, sceHCD, ETD, and EThcD has not been reported.

Here, we systematically explore the advantages and disadvantages of sceHCD and EThcD for intact glycopeptide analysis, put the methods in context with their canonical HCD and ETD counterparts, and comment on their suitability for both *N*- and *O*-glycoproteomic applications. We test 14 product-dependent triggering methods (i.e., HCD-pd-X, where X is an MS/MS dissociation type) and also evaluate several HCD-pd-X methods relative to traditional data-dependent acquisition (DDA). We compare standard HCD, sceHCD, ETD, and EThcD for tryptic *N*-glycopeptides generated from a panel of glycoprotein standards, in addition to *N*-glycopeptides enriched from tryptic digests of HEK 293 whole cell lysates. We also test each method using *O*-glycopeptides generated with the recently characterized mucinase, StcE, to comment on *O*-glycoproteomic performance.[89] In all, we show that while HCD and sceHCD are sufficient for most *N*-glycoproteomic applications, they are ill-suited for site-specific *O*-glycoproteomic analysis. Instead, EThcD is the premier choice for *O*-glycopeptide characterization, despite excitement about the potential of sceHCD. We also discuss how these results affect continued efforts toward improving our analytical toolkit, including choices of instrument platforms and software development for data analysis.

EXPERIMENTAL SECTION

A standard glycoprotein mixture, a pool of *N*-glycopeptides enriched from HEK293 whole cell lysate, and a mixture of recombinant mucins were analyzed using multiple MS/MS dissociation methods. The standard glycoprotein mixture consisted of eight glycoproteins: bovine fetuin (P12763), bovine alpha-1-acid glycoprotein (Q3SZR3), recombinant human hemopexin (P02790), recombinant human CD14 (P08571), human fibronectin (P02751), human plasma protease C1 inhibitor (C1inh) (P05155), recombinant human CD59 (P13987), and recombinant human platelet glycoprotein 1b alpha (GP1ba) (P07359). Figure S1 depicts glycosites in these standard glycoproteins. Twenty micrograms of each protein was combined prior to tryptic digestion, and approximately 2 μg of total peptide was injected per LC−MS/MS analysis. HEK293 cells were lysed, 1 mg was digested with trypsin using an S-trap protocol,[90] and glycopeptides were enriched using an SAX-ERLIC solid-phase extraction method[24] prior to LC−MS/MS. The mucin mixture consisted of recombinant human GP1ba (P07359), recombinant human leukosialin (CD43) (P16150), recombinant human MUC16 (Q8WXI7.3), and recombinant human P-selectin glycoprotein ligand 1 (PSGL1) (Q14242). Proteins (10 μg each) were digested individually similar to previously described methods using a 3 h StcE digestion, followed by an overnight PNGaseF incubation and a 12 h tryptic digestion.[89] After digestion, peptides were combined in equal parts by mass for the four proteins and analyzed by LC−MS/MS (approximately 2 μg total peptides per injection). Fourteen product-dependent methods were constructed using different dissociation types as the triggered scan, i.e., HCD-pd-X, where X is a dissociation type defined in Figure 1a. The numbers used in all methods indicate normalized collision energy (nce) settings used for collisional dissociation, and "A ± B" values for sceHCD methods indicate the central nce (A) and the step size (B) in either direction from

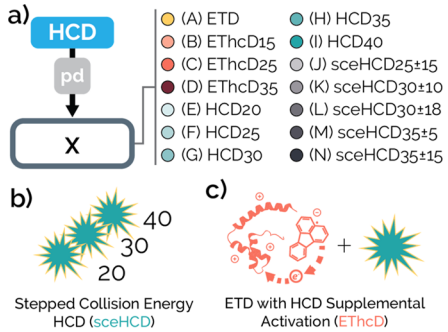

Figure 1. Comparing glycopeptide dissociation methods for *N*- and *O*-glycopeptides. (a) Several product-dependent (pd) methods, i.e., HCD-pd-X, were constructed to investigate glycopeptide fragmentation quality, where X refers to different the dissociation types shown. We compared ETD, EThcD with several collision energies, several conventional HCD collision energies, and several stepped collision energy (sce) HCD methods, where the number after the method indicates the normalized collision energy used and "±" in sceHCD methods indicates the step size in energy from the center value provided. Each method has an assigned letter (A−N), which is used for identification in subsequent figures. Schematics illustrate (b) sceHCD30 ± 10 and (c) EThcD fragmentation prior to mass analysis.

https://dx.doi.org/10.1021/acs.jproteome.0c00218
J. Proteome Res. 2020, 19, 3286−3301

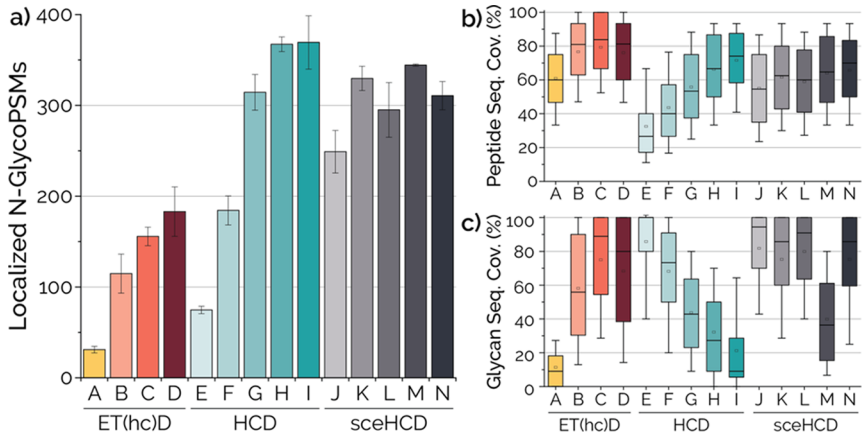

Figure 2. Collision-based methods are sufficient for *N*-glycopeptides. (a) Average number of localized *N*-glycopeptide spectral matches (*N*-glycoPSMs) is shown for technical triplicate analyses of tryptic peptides generated from a mixture of eight glycoproteins. Error bars show one standard deviation. Box plots show the distribution of (b) peptide backbone sequence coverage (i.e., the proportion of peptide backbone bonds that can be explained by fragment ions) and (c) glycan sequence coverage (i.e., the proportion of glycosidic bond cleavages observed) for *N*-glycopeptides identified with each method. Letters on the *x*-axes (A−N) correspond to the labels in Figure 1 and are grouped by method type.

the central value. To construct these methods, we explored nine HCD collision energies individually to understand how each collision energy used in standard HCD and sceHCD contribute to performance (Figure S2). (Glyco)peptide mixtures were separated using an Easy-Spray column packed with C18 PepMap material and a Dionex UltiMate 3000 LC pump. All LC−MS/MS methods were 90 min total, and each method was run in technical triplicate, except for the HEK293 glycopeptides, which we only injected once per dissociation method. Scout HCD scans used a normalized collision energy of 36, a resolving power of 30,000 at 200 m/z, and an automatically determined scan range (Auto Normal) calculated based on precursor m/z with the first mass set to 100 m/z. Triggered MS/MS scans utilized the Orbitrap high mass range (120 to 4000 m/z), which has been shown to benefit glycopeptide analysis,[91] and a resolving power of 30,000. ETD and EThcD methods used calibrated charge-dependent parameters for calculating reagent AGC targets and ion−ion reaction times.[92] Product-dependent triggering required at least two ions from the following list to be present in the top 20 most abundant peaks in a spectrum within a 25 ppm tolerance: 126.055, 138.0549, 144.0655, 168.0654, 186.076, 204.0865, 274.0921, 292.1027, and 366.1395 m/z. Several 90 min standard DDA methods were also tested, where the desired dissociation method was used for all precursors without a scout HCD or triggering event. All raw data were searched using Byonic.[93] For the standard glycoprotein mix, *N*- and *O*-glycopeptide searches were conducted separately,[94] each using the same fasta sequence file specific to the mixture. Glycopeptides from the HEK293 lysate were searched using a focused database[95] created from prior data-dependent proteomic analyses. Mucin *O*-glycopeptides were searched using a specific mucin fasta sequence file. The *N*-glycan database for both the standard glycoprotein mixture and HEK293 *N*-glycopeptide searches consisted of 286 unique compositions of which HexNAc(1) was not included. The *O*-glycan database used for *O*-glycopeptide searches consisted of nine common *O*-glycans. After Byonic searches, result files were filtered and fragmentation statistics were calculated using scripts written in C# using the C# Mass Spectrometry Language (CSMSL, https://github.com/dbaileychess/CSMSL). Filtering Byonic search results is necessary to retain only high-quality identifications and minimize false positives.[96] Filtering metrics included a Byonic score greater than or equal to 200, a logProb value greater than or equal to 2, and a peptide length greater than 4 residues. A maximum of three glycosites were allowed for any one glycopeptide. Data was graphed using OriginPro 2018. For box plots, median and quartile values are provided by the center line and box boundaries, respectively. Whiskers show 10th and 90th percentiles, and the small square indicates the average. More method details are available in the Supporting Information.

RESULTS AND DISCUSSION

We systematically compare HCD, sceHCD, ETD, and EThcD for their performance in characterizing intact *N*- and *O*-glycopeptides. With variations in normalized collision energies among these four dissociation types, we created 14 product-dependent methods. Figure 1a shows the method structure we chose for comparing these methods, where we use product-dependent triggering to maximize the time spent on glycopeptide analysis. In these HCD-pd-X methods, a scout HCD scan provides product ions from collisional dissociation of precursors in a data-dependent fashion. The presence of glycopeptide-specific oxonium ions (see Experimental Section and Supporting Information) then triggers a scan of specific dissociation type X to fragment the glycopeptide, where X is one of the 14 methods shown. Note that the letters next to each method are used as identification codes in subsequent figures. Figure 1b,c depicts sceHCD and EThcD scan events, respectively, to illustrate what happens to ions prior to mass analysis. We consider several figures of merit beyond merely numbers of identifications as we compare methods, including (1) degree of peptide backbone sequence coverage, (2) degree of glycan sequence coverage, (3) proportion of signal in different fragment ion types (i.e., oxonium ions, Y-type ions, and peptide backbone fragment ions), (4) percentage of spectra that enable confident glycosite localization, (5) percentage of spectra that contain fragments with glycans (intact or fragments) retained, and (6) proportions of total ion current that can be confidently annotated/explained in identified spectra. In order to ensure quality identifications, glycopeptide spectral matches (glycoPSMs) returned from Byonic for all methods were filtered to have a Byonic score greater than or equal to 200, a logProb

https://dx.doi.org/10.1021/acs.jproteome.0c00218
J. Proteome Res. 2020, 19, 3286−3301

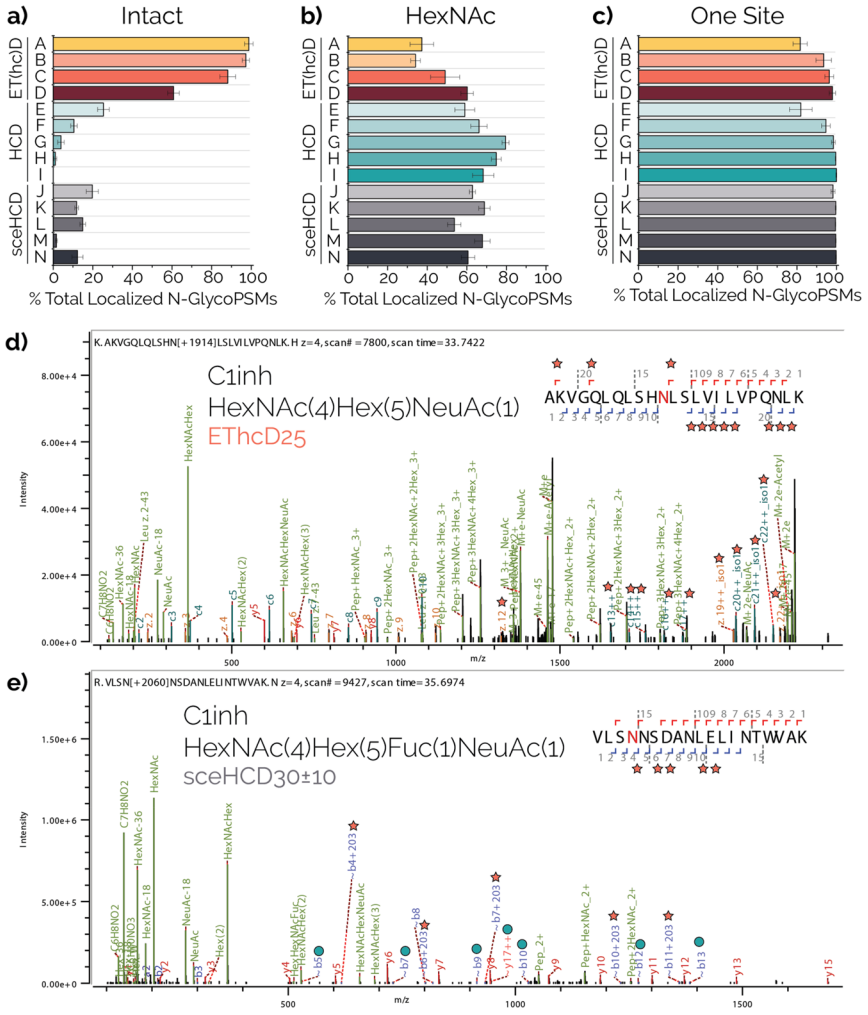

Figure 3. Evidence for localized glycosites in *N*-glycopeptides. Three panels at the top provide the percentage total localized identifications that can be explained using (a) intact peptide backbone fragments (i.e., that have no glycan neutral losses), (b) peptide backbone fragments that retain the +203.0794 Da mass shift to indicate a remaining HexNAc fragment, or (c) presence of only one potential *N*-glycosite (i.e., one N-X-S/T sequon). Letters on the *y*-axes (A−N) correspond to the labels in Figure 1 and are grouped by method type. (d) Example of localization using intact fragments in an EThcD25 spectrum (precursor *m*/*z*: 1107.2990, *z*: 4). Ions with a red star are important for localization, the majority of which retain the intact glycan mass. (e) Example of localization using HexNAc-retaining (+203.0794) fragments in a sceHCD30 ± 10 spectrum (precursor *m*/*z*: 1040.9621, *z*: 4). Red stars show peptide ions that usefully retain the HexNAc moiety to show where the glycosite is. Blue circles indicate peptide fragments that did not retain the HexNAc mass and are not useful for localization, a common phenomenon in HCD and sceHCD spectra. Note, a fragment with a "∼" denotes a peptide backbone fragment that does not retain any glycan, and both panels (d) and (e) show tryptic peptides from C1inh. Byonic color coding of annotated fragments show *N*-terminal peptide fragment ions in blue, *C*-terminal peptide fragment ions in red, and glycan-derived fragment ions in green.

score greater than or equal to 2, and a peptide length equal to five residues or greater.

N-Glycopeptides

The average number of localized *N*-glycopeptide spectral matches (*N*-glycoPSMs) for each method is summarized in Figure 2a. Localization here, and throughout this work, is defined as the unambiguous assignment of a glycosite within a glycopeptide (discussed further below). The advantage for generating identifications is clear for HCD and sceHCD methods, and both HCD35 and HCD40 outperform sceHCD methods in terms of identification numbers. Looking at peptide sequence coverage and glycan sequence coverage in Figure 2b,c, however, it is clear that HCD methods sacrifice peptide fragmentation quality for glycan fragmentation quality or vice versa, while sceHCD methods provide quality fragmentation for both moieties. sceHCD30 ± 10, sceHCD30 ± 18, and sceHCD35 ± 15 all provide good peptide and glycan sequence coverage with similar identification numbers, with a slight identification advantage for sceHCD30 ± 10. EThcD15, EThcD25, and EThcD35 all generate superior peptide sequence coverage for all methods, and EThcD25 also excels at glycan fragmentation. However, ETD and EThcD scans are significantly slower than HCD and sceHCD scans, resulting in fewer MS/MS acquisitions (Figure S3). This speed issue limits their effectiveness compared to the collision-based alternatives despite the superior fragmentation quality.

We next compared the types of localization evidence each method generated for *N*-glycosites (Figure 3). There are three ways to localize glycosites: (1) intact fragments, where peptide backbone fragments retain glycan moieties to enable unambiguous glycosite assignment; (2) HexNAc-retaining fragments, where peptide backbone fragments lose most of the glycan moiety but retain the initiating HexNAc monosaccharide for a

https://dx.doi.org/10.1021/acs.jproteome.0c00218
J. Proteome Res. 2020, 19, 3286−3301

mass shift of +203.0794 Da (for *N*-glycopeptides, this is a GlcNAc residue) to show which amino acid harbored the glycan; and (3) the presence of only one potential glycosite in the peptide sequence. More than 90% of the total *N*-glycoPSMs that passed the post-Byonic filtering were localized successfully for EThcD methods, sceHCD methods, and HCD30-40 methods (Figure S4a). Figure 3a shows that the majority (>∼90%) of localized *N*-glycoPSMs from ETD, EThcD15, and EThcD25 spectra have evidence for localization via intact (c/z·-type) fragments, compared to only ∼60% of EThcD35 localized *N*-glycoPSMs. Recent work has shown that the site of glycan attachment and the glycan itself can affect localization with ETD.[97,98] Here, we see that EThcD methods identify *N*-glycopeptides with glycosites distributed more evenly across the peptide backbone (Figure S5), potentially mitigating some glycan/glycosite localization dependency of ETD.

HCD methods steadily decrease their proportion of b/y-type fragments that retain intact glycans as collision energies increase, while sceHCD25 ± 15 generates the most localized *N*-glycoPSMs with intact glycan-retaining fragments (∼20% of spectra), followed by sceHCD30 ± 10. On the other hand, HCD30 provides the largest proportion of *N*-glycoPSMs that can be localized with HexNAc-retaining fragments (∼80%), and sceHCD30 ± 10 and sceHCD35 ± 5 are highest of the sceHCD methods (just under ∼70%) (Figure 3b). Regardless of the spectral evidence provided by intact or HexNAc-retaining peptide backbone fragments, the majority (>93%) of all *N*-glycoPSMs could be localized purely in the presence of only one *N*-glycosite, except for ETD and HCD (∼82% each), meaning that little spectral evidence is needed for a confident localization (Figure 3c). That said, *N*- and *O*-glycosites can be contained within the same glycopeptide, which would confound this one glycosite assumption and would thus require spectral evidence for localization. Furthermore, for longer glycopeptides that are characterized using middle-down approaches, the presence of multiple *N*-glycosites necessitates the use of electron-driven activation to generate intact fragments to properly localize each glycan.[99] Only a handful of *N*-glycoPSMs here were identified with multiple *N*-glycosites (mostly using ETD-based methods), with approximately five identifications having spectral evidence to localize both glycan modifications (Figure S6). In this dataset, >90% of ETD, EThcD15, and EThcD25 localized *N*-glycoPSMs have spectral evidence for localization (i.e., intact and/or HexNAc-retaining peptide backbone fragments), while only ∼60−80% of localized *N*-glycoPSMs are supported by spectral evidence for EThcD35, HCD methods, and sceHCD methods (Figure S4b). Example spectra from C1inh-derived *N*-glycopeptides with similar glycan modifications illustrate the two different special evidence types, i.e., intact fragments in EThcD25 (Figure 3d) and HexNAc-retaining fragments in sceHCD30 ± 10 (Figure 3e).

Figure S7 illustrates the number of different product ion types each method generates in *N*-glycoPSMs, including peptide backbone fragments, peptide backbone fragments that have a glycan neutral loss, peptide backbone fragments that retain a HexNAc moiety, Y-type ions (which represent an intact peptide attached to a fragment of the original glycan broken along glycosidic bonds), and oxonium/ B-type ions that represent only glycan moieties. Note that "peptide backbone fragments" include both those that are not expected to harbor a glycan and those that are seen with an intact glycan, while "glycan neutral loss fragments" include peptide fragments that have fully lost the glycan or retain only a HexNAc remnant. Interestingly, while peptide backbone fragments retaining the intact glycan mass can be observed in HCD and sceHCD, they are far more the exception than the rule (Figure S7b). Peptide fragments retaining the intact glycan are readily observed in ETD and EThcD spectra but become less frequent as supplemental HCD collision energy increases in EThcD. Also, while Y-type fragments can be useful for indicating some glycan structural information, some Y-type ions observed here are likely the result of more than one glycosidic cleavage, which are not as useful or reliable for structural determination. ETD and EThcD methods generate more peptide backbone fragments, with a small fraction of HexNAc-remnant fragments being present, while HCD and sceHCD methods can produce nearly as many neutral loss fragments as standard peptide fragments. Approximately half of the neutral loss fragments in HCD and sceHCD spectra are HexNAc-remnant fragments, although this differs slightly based on the method. Figure S8 summarizes these distributions by comparing the median number of fragments for each method, delineated by fragment type. The trends in numbers of fragments explain the sequence coverages seen in Figure 2, and they translate to the amount of explainable signal (total ion current) in spectra from each dissociation type (Figure S9). Figure S10 shows the distribution of explainable signal between four different fragment types. EThcD 25 distributes signal between peptide backbone fragments, Y-type ions, and oxonium ions most evenly of any dissociation method while also minimizing the signal from peptide backbone fragments with neutral losses. The majority of signal in HCD and sceHCD spectra is in glycan-related channels, i.e., Y-type fragments and oxonium ions, although peptide backbone fragment signal generally increases with higher collision energies. In general, EThcD methods provide the highest quality fragmentation.

We repeated our comparison of methods for *N*-glycopeptides enriched from HEK293 whole cell lysate using eight of the methods tested for the standard glycoprotein mixture. Figure 4a shows the number of *N*-glycoPSMs identified for the eight methods, and it also provides a comparison to standard DDA analyses for two HCD and two sceHCD methods. The superior performance of the HCD and sceHCD is again evident, but perhaps more striking is the significantly higher number of identifications with standard DDA methods compared to product-dependent methods. One reason for this is that the identifications in the scout HCD scans in HCD-pd-X methods have not been included in our results so far (as to not confound data interpretation of each individual method), which removes one-third to one-half of total *N*-glycoPSMs. Figure 4b demonstrates that the two approaches are more evenly matched when also including *N*-glycoPSMs from scout HCD scans, although the standard DDA methods still have the slight advantage. Note that the advantages of fragmentation quality, especially for sceHCD methods, are not applicable to the identifications from scout HCD scans. These results highlight that product-dependent methods may not be necessary in samples that have been enriched for *N*-glycopeptides; the majority of precursors in such samples are glycopeptides, and thus screening precursors via the scout HCD scan is unnecessary. This does not hold true for the standard glycoprotein mix, where HCD-p-X methods significantly outperform standard DDA methods (Figure 4c). The standard glycoprotein mixture was not enriched, meaning that many nonglycosylated peptides are present along with glycopeptides. This discrepancy highlights how product-dependent methods are advantageous for samples with low *N*-glycopeptide enrich-

https://dx.doi.org/10.1021/acs.jproteome.0c00218
J. Proteome Res. 2020, 19, 3286−3301

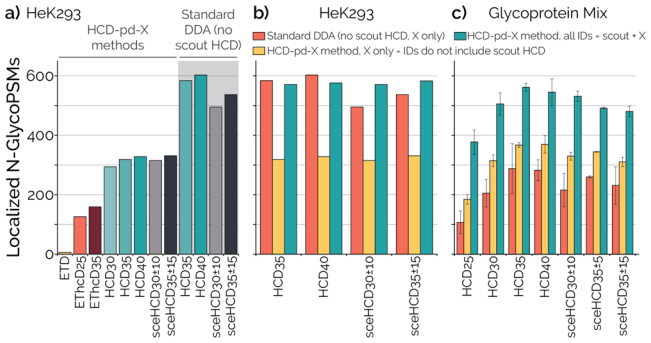

Figure 4. Trends hold true for *N*-glycopeptides enriched from complex lysate, but HCD-pd-X methods are not always necessary. (a) Numbers of localized *N*-glycoPSMs from glycopeptides enriched from HEK293 whole cell lysate are shown for a select number of HCD-pd-X experiments. Also shown are four methods where product-dependent triggering was not used, but instead, the dissociation method was used for every precursor (i.e., a standard DDA method, gray box). (b) Numbers of localized *N*-glycoPSMs from enriched HEK293 lysate are shown for standard DDA methods (red) and for HCD-pd-X methods, where identifications are delineated as including only those from X fragmentation (yellow) or from both the scouting HCD and X spectra (blue). (c) Same comparison as in panel (b) of standard DDA and HCD-pd-X methods is shown for localized *N*-glycoPSMs from the mixture of standard glycoproteins. Note that the *y*-axes for all three panels are the same, with the definition at the left, and the three-color legend is only for panels (b) and (c).

ment efficiency (i.e., where little to no enrichment is performed), but they are not always necessary for high enrichment efficiency samples. In all, our data from both the standard glycoprotein mixture and the HEK293 *N*-glycopeptides show that HCD and sceHCD methods are sufficient for standard *N*-glycoproteomics, despite the superior spectral quality of EThcD methods.

O-Glycopeptides

We first searched the standard glycoprotein mixture data set for *O*-glycopeptides because several of these glycoproteins are known to have *O*-glycosites. While some spectra, especially EThcD spectra, were confidently identified, the number of localized *O*-glycoPSMs was lower than desired to draw conclusions (Figure S11). Instead, we opted to generate a new sample for *O*-glycopeptide interrogation using the professional mucinase, StcE, which cleaves specifically in glycosylated mucin domains.[89] StcE is particularly important for characterizing densely *O*-glycosylated mucin proteins because mucin domains are largely impervious to other proteases. Canonical proteolysis of mucins (e.g., with trypsin, chymotrypsin) generates *O*-glycopeptides tens to hundreds of residues in length, comprising mostly serine, threonine, and proline residues (so-called PTS domains). Furthermore, the majority of serine and threonine residues in these stretches are *O*-glycosylated. These *O*-glycopeptides are effectively impossible to sequence at all, much less with any site specificity of *O*-glycosite localization. StcE recognizes glycosylated serine and threonine residues in these PTS domains, cleaving to produce *O*-glycopeptides more amenable to MS analysis. Using PNGaseF to deglycosylate *N*-glycosites and a combination of StcE and trypsin for peptide backbone proteolysis, we digested four recombinant mucins and analyzed them with 12 HCD-pd-X methods (Figure 5). Contrary to the *N*-glycopeptide analysis above, EThcD significantly outperformed all other methods for *O*-glycopeptide identification (Figure 5a), even with similar differences in acquisition rate seen in the *N*-glycopeptide data set (Figure S3). Surprisingly, peptide sequence coverage was consistently good across EThcD, HCD, and sceHCD data for *O*-glycopeptide spectra (Figure 5b). Glycan sequence coverage was moderate for EThcD and HCD methods, was nonexistent for ETD (which generates virtually no Y-type fragments), and was most favorable for sceHCD methods except sceHCD35 ± 5 (Figure 5c).

The superior performance of EThcD was enabled by the retention of intact glycan moieties on peptide backbone fragment ions (Figure 6). ETD, EThcD, HCD, and sceHCD all produced sufficient numbers of peptide backbone fragments (Figure 5b, Figure S7a), but the majority of HCD and sceHCD peptide fragments had glycan neutral losses (Figure S7b). In contrast, ∼99% of localized *O*-glycoPSMs could be localized using intact peptide backbone fragments for ETD, EThcD15, and EThcD25 (∼94% for EThcD35). While some HexNAc-retaining fragments were detected in EThcD, HCD, and sceHCD spectra (Figure S7c), these are often not sufficient for glycosite localization in *O*-glycopeptides because multiple

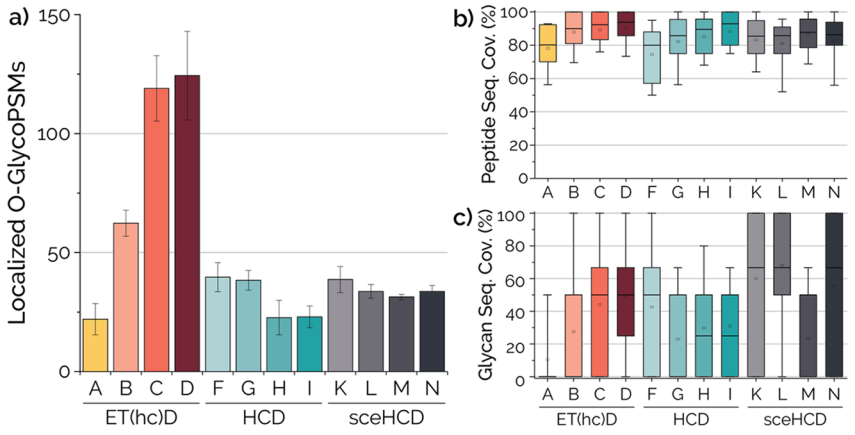

Figure 5. EThcD methods are significantly better at *O*-glycopeptide characterization. (a) Average number of localized *O*-glycopeptide spectral matches (O-glycoPSMs) is shown for *O*-glycopeptides generated from four recombinant mucin glycoproteins after enzymatic treatment with PNGaseF, trypsin, and StcE. Error bars show one standard deviation. Box plots show the distribution of (b) peptide backbone sequence coverage and (c) glycan sequence coverage for *O*-glycopeptides identified with each method. Letters on the *x*-axes (A−D, F−I, and K−N) correspond to the labels in Figure 1 and are grouped by method type.

https://dx.doi.org/10.1021/acs.jproteome.0c00218
J. Proteome Res. 2020, 19, 3286−3301

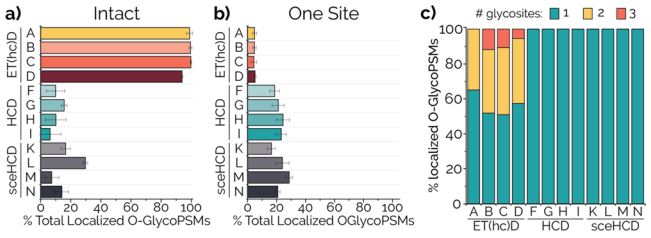

Figure 6. *O*-glycopeptides require localization using intact fragments, which enables localization of multiple *O*-glycosites per peptide. (a) Percentage of total localized *O*-glycopeptide identifications that can be explained using intact peptide backbone fragments. (b) Percentage of total localized *O*-glycopeptide identifications that can be explained by the presence of only one potential *O*-glycosite. (c) Proportions of localized *O*-glycoPSMs that were identified with one, two, or three glycosites. Letters (A–D, F–I, and K–N) on the *y*-axes for panels (a) and (b) (and on the *x*-axis for panel (c)) correspond to the labels in Figure 1 and are grouped by method type.

serine and/or threonine residues lead to ambiguity. This is further supported by the lower percentage of *O*-glycoPSMs that could be localized due to the presence of only one potential glycosite (Figure 7b). This is largely expected for *O*-glycopeptides derived from mucins, which have dense regions of glycosylation and repeating domains rich in serine and threonines, but 68% of tryptic peptides from the standard glycoprotein mixture also harbor more than one serine or threonine (Figure S12b), indicating that this is a phenomenon common to *O*-glycopeptides. Consequently (and similarly to *N*-glycopeptides, Figure S6), multiply glycosylated *O*-glycopeptides were detected in ETD and EThcD methods while the *O*-glycopeptides that were identified by HCD and sceHCD were exclusively singly modified species (Figure 6c).

Figure 7 provides an illustrative example of how HCD fails and EThcD succeeds at characterizing *O*-glycopeptides. The peptide TKPVSLLESTKKTIPELDQPPK from platelet glycoprotein 1b alpha (GP1ba, CD42) is the result of combined StcE and trypsin cleavage at the N- and C-terminus, respectively. HCD and sceHCD spectra generate high scoring spectral matches that have numerous peptide backbone fragments (Figure 7a), but all of the b/y-type fragments that would explain the assigned glycosites are missing glycan modifications (as indicated by the "~" symbol). The correct total glycan composition, HexNAc(2)Hex(2)NeuAc(3), is assigned to the sequence but the localization assignments are entirely incorrect. An EThcD spectrum of the same precursor shows extensive peptide backbone fragmentation, and the peptide fragments retain intact glycan(s) (Figure 7b). This spectral evidence enables confident, unambiguous assignment of glycan compositions to two threonine sites (indicated in red). The need for unambiguous glycosite assignment is further emphasized by the presence of multiple glycoforms of this peptide, as shown in Figure 7c,d. EThcD correctly localizes glycans, including a disialylated core-1 structure, to three different glycosites in different glycoforms. HCD and sceHCD are blind to the locations of each glycan, making glycoform analysis impossible, whereas EThcD has the ability to assign site specificity even for multiply sialylated *O*-glycopeptides. We did not see evidence for positional isomers of the reported glycopeptides in these spectra, but multiple glycoforms of the same peptide sequence can complicate spectral interpretation. This underscores the need for continued development of analysis tools to interpret complex glycopeptide spectra resulting from multiple glycoforms. Note that *O*-glycan structures were not determined from the spectra but rather depict the most common structures known for these glycans (with linkage information purposefully omitted). Interestingly, GP1ba was also in the standard glycoprotein mixture that was digested with trypsin only. In that data set, where only a handful of localized *O*-glycopeptides were confidently identified, EThcD provided localized *O*-glycoPSMs only for singly glycosylated *O*-glycopeptides from this same region of GP1ba. The ability to confidently characterize the doubly and triply glycosylated species in the StcE+trypsin mucin *O*-glycopeptide mixture highlights the value StcE adds to *O*-glycoproteomic workflows.

Our data shows that HCD and sceHCD are generally not reliable at generating fragment ion types sufficient for robust *O*-glycopeptide characterization. This shortcoming of HCD and sceHCD for *O*-glycopeptides is underscored by the reliance on ETD-based methods for *O*-glycopeptides even when *O*-glycans are simplified to truncated forms, i.e., the SimpleCell system,[100−105] and by the lack of ability to localized the *O*-glycopeptide spectra in limited previous studies investigating *O*-glycopeptides with HCD and sceHCD spectra.[69,79,87] Some studies have reported the retention of *O*-glycans on b/y-type peptide backbone fragments during collision-based *O*-glycopeptide fragmentation.[76,106] Indeed, the tens of *O*-glycoPSMs localized by HCD and sceHCD methods in this study were able to be localized mainly due to HexNAc-retaining b/y-type ions (which is an *N*-acetylgalactosamine, or GalNAc, residue in mucin-type *O*-glycopeptides). However, this represents less than ~8−15% of the total *O*-glycoPSM identifications retained after post-Byonic filtering for HCD and sceHCD methods, compared to a ~65% localization rate of total *O*-glycoPSMs for EThcD25 (Figure S12a). Others have used HCD in combination with trypsin and proteinase K or pronase proteolysis to make short peptides with few possible glycosites with some success.[107−109] While this strategy may be effective at generating short glycopeptides that can be successfully characterized with HCD, nonspecific digestions create issues with database searching, both in increasing search space and time requirements and also in increased rates of false identifications. Thus, the more straightforward approach is to utilize EThcD methods. A recent development that may mitigate this requirement is the *O*-glycoprotease called OpeRATOR, which cleaves the N-terminal residue.[110,111] This is an exciting proposition that could have significant impact on *O*-glycoproteomic methods, allowing researchers to capitalize on the benefits of HCD and sceHCD methods. That said, *O*-glycoproteomic applications with OpeRATOR likely need further testing to understand how many missed cleavages occur that would create internally glycosylated residues to confound localization in HCD or sceHCD spectra.

Comparisons between *N*- and *O*-Glycopeptide Data

Beyond the intraclass comparison of methods for *N*- and *O*-glycopeptide mixtures, our data allows comparisons across data sets to identify spectral features inherent to each class of glycopeptide. Perhaps one of the most intriguing differences between *N*- and *O*-glycopeptides is the generation of peptide backbone fragments under different conditions. *N*-glycopeptides show a dependency on collision energy for the number of peptide sequencing ions generated (Figure S6) and the subsequent peptide sequence coverage achieved (Figure 2b). *O*-glycopeptides, on the other hand, generate a larger number of peptide backbone fragments than *N*-glycopeptides (Figures S7

https://dx.doi.org/10.1021/acs.jproteome.0c00218
J. Proteome Res. 2020, 19, 3286−3301

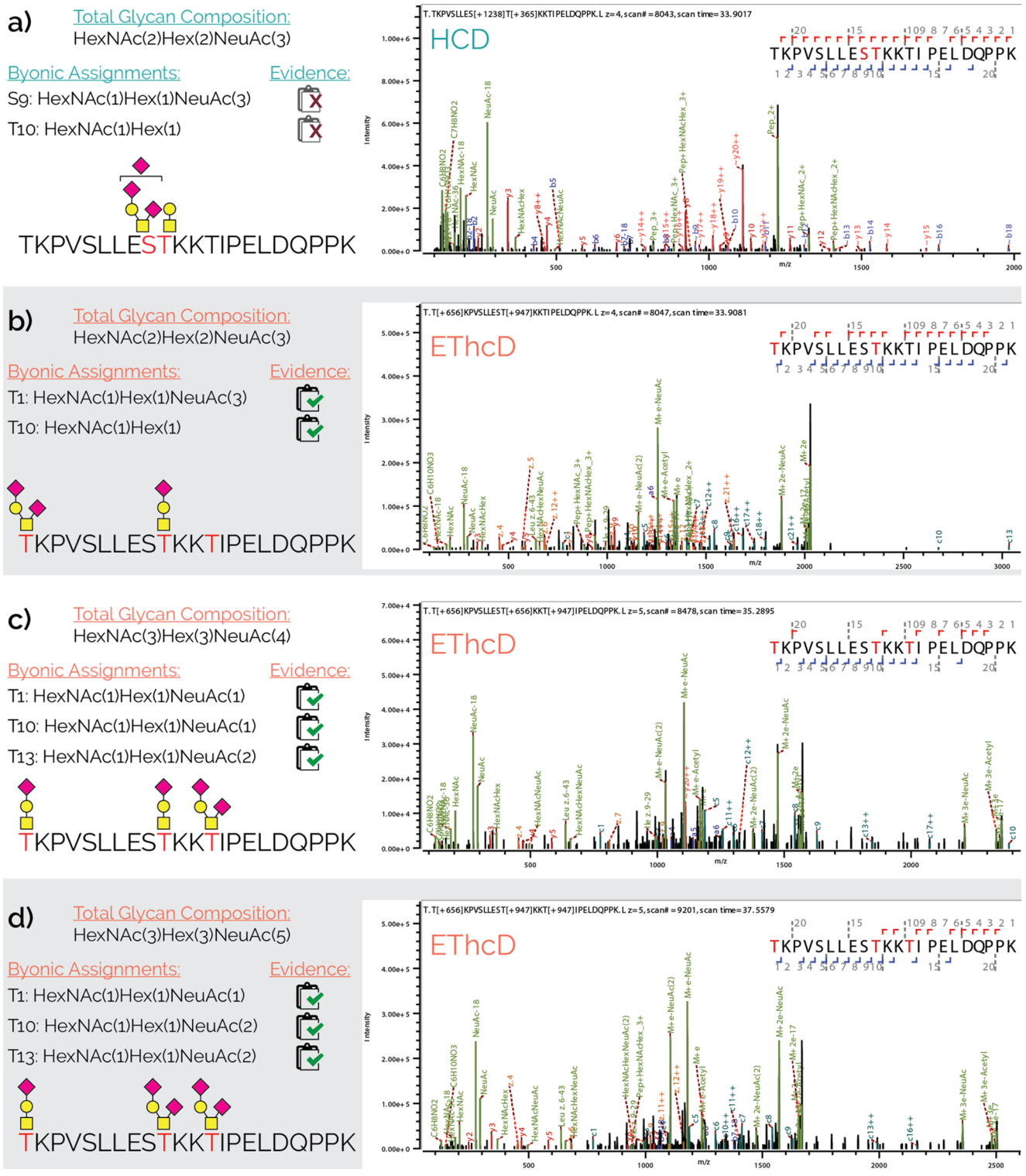

Figure 7. Examples of why HCD fails and EThcD succeeds at *O*-glycosite localization. The peptide sequence TKPVSLLESTKKTIPELDQPPK, generated by combined StcE and trypsin cleavage of GP1b alpha, was detected with many different glycoforms in all methods. For HCD methods, the glycosites and respective glycan compositions were defined without any spectral evidence, as exemplified in panel (a), leading to incorrect localization (precursor m/z: 1014.4911, z: 4). No localized glycoPSM of this precursor was identified in any HCD or sceHCD analyses. Note that a fragment with a "~" denotes a peptide backbone fragment that does not retain any glycan. Panel (b) is an EThcD spectrum of same precursor, where two glycosites are confidently localized with defined glycan masses based on direct observation of intact peptide backbone product ions. Panels (c) and (d) show the EThcD spectra of different precursors (precursor m/z: 943.0402, z: 5; and precursor m/z: 1001.4602, z: 5, respectively) that provide confident localization of three glycosites in same peptide sequence with different combinations of glycans, highlighting the need for localization in *O*-glycopeptide characterization. Annotation labels follow the same scheme as noted as the end of Figure 3.

https://dx.doi.org/10.1021/acs.jproteome.0c00218
J. Proteome Res. 2020, 19, 3286−3301

and S8) and have higher peptide sequence coverage values, with less variation based on collision energy or HCD versus sceHCD (Figure 5b). More peptide backbone fragments retaining intact glycan masses were observed in EThcD spectra of *O*-glycopeptides compared to *N*-glycopeptides, which is likely because more glycosites are present throughout peptide sequence (Figure 6c and Figures S6 and S7). The number of neutral loss-associated peptide backbone fragments was also greater for *O*-glycopeptides, including EThcD methods. This supports a recent report by Kelly and Dodds, where they found that *O*-glycopeptides require lower collision energies for precursor depletion for a small pool of *O*-glycopeptides.[88] Although some increase in the number of neutral loss-associated backbone fragments can likely be attributed to the greater number of potential glycosites, this also shows that the dissociation thresholds for GalNac-Ser/Thr may be lower than GlcNAc-Asn. Conversely, *N*-glycopeptides generated more Y-type and oxonium/B-type ions than *O*-glycopeptides, likely explained by the larger size of *N*-glycans.

Figures S14−S16 provide distributions of precursor peptide lengths, m/z values, and charge state distributions of identified *N*- and *O*-glycoPSMs for each method. As expected, EThcD methods extend the m/z range of ETD for successfully identified glycopeptides, making their distributions more similar to HCD and sceHCD methods. Peptide lengths of identified glycopeptides are generally similar between the different methods, and identified *O*-glycopeptides tend to be slightly longer than *N*-glycopeptides on average. Even though all methods across both glycopeptide classes had the same settings for precursor charge state selection, fewer $z = 2$ *N*-glycopeptides were identified relative to *O*-glycopeptides while more highly charged *N*-glycopeptides were sequenced. This observation could be both peptide sequence-dependent (as *O*-glycopeptides tend to be less enriched for basic residues) and glycan-dependent (as smaller *O*-glycans are less likely to carry a positive charge). The majority of identifications from HCD and sceHCD methods for both classes of glycopeptides were $z = 3$ precursors, although this was generally more prevalent for *O*-glycopeptides, while ETD-based methods broadened the charge state distributions of *N*- and *O*-glycoPSMs.

Given these complementary trends in peptide and glycan fragment generation, the amount of signal that could be explained for the different fragmentation methods was approximately the same for both classes (Figure S9). The distribution of that signal, however, varied greatly between *N*-glycopeptides (Figure S10) and *O*-glycopeptides (Figure S13). HCD and sceHCD spectra of *N*-glycopeptides were dominated by oxonium ions, and the proportion of Y-type ion signal steadily decreased with increasing collision energy, accompanied by an increase in peptide backbone fragment signal. HCD and sceHCD of *O*-glycopeptides had more balanced signal distributions, with noticeably larger proportions of peptide backbone fragments that had neutral losses. *N*-glycopeptide EThcD spectra had more signal occupied by oxonium ions and Y-type ions at higher collision energies, while *O*-glycopeptide EThcD spectra had more than half of their signal in peptide fragment channels. Again, this is likely due to larger *N*-glycans compared to *O*-glycans, but these are important spectral features to consider when developing algorithms to score *N*- and *O*-glycopeptide spectra. The Delta Mod score, which is the drop in Byonic score from the top-scoring identification to the second-best identification, showed drastically different distributions for *N*- and *O*-glycopeptides (Figure S17). According to Byonic documentation, Delta Mod scores below 20 indicate dubious modification site assignments while scores above 40 mean that the reported identification is significantly better than other candidates. These distributions further support the relative ease of localizing *N*-glycopeptides with both sceHCD and EThcD methods (albeit with different levels of confidence) compared to the challenge of *O*-glycosite localization.

Despite the evidence of higher quality spectra for EThcD for both *N*- and *O*-glycopeptides, Byonic appears to under-score EThcD spectra relative to HCD and sceHCD for both classes (Figure S18). For each glycopeptide identification, we compared the best scoring scout HCD scan to the best scoring spectrum from triggered dissociation methods. EThcD spectra had a higher score than scout HCD spectra for only 45−55% of *N*-glycopeptide identifications. Comparatively, HCD35 and HCD40 outscore their scout HCD scans 86 and 93% of the time, and the sceHCD30 spectra outscore ∼70−90% of their corresponding scout HCD spectra. The problem is even more exacerbated for *O*-glycopeptides, where EThcD25 and EThcD35 outscore scout HCD spectra only ∼10 and ∼32% of the time, compared to >75% for most HCD and sceHCD methods. This is likely because Byonic was not designed specifically for glycopeptide spectral analysis, weights high intensity matching fragments favorably, and rewards the presence of expected fragments (even b/y-type fragments that have complete glycan loss),[112] which may give an unfair advantage to HCD spectra over ETD and EThcD. Regardless, this highlights the need to incorporate spectral features specific to glycopeptide dissociation as search algorithms continue to progress. Such changes could include weighting peptide backbone fragments that retain an intact glycan or HexNAc moiety as the most important matched peaks in a spectrum. This could allow more nuanced analyses of glycoforms and the presence of multiple positional isoforms present within the same spectrum. Localization algorithms that leverage this type of information are widely used in phosphoproteomics[113] but have remained largely absent in glycoproteomics. Considering the general lack of structural information derived from the majority of intact glycopeptide studies, peptide fragment scores should likely be weighted more heavily than Y-type ions (and certainly more heavily than oxonium ions, regardless their abundance).

Even so, Y-type ions can be useful and are known features of glycopeptide HCD and sceHCD spectra, especially Y1 ions (peptide+GlcNAc) in *N*-glycopeptide spectra and Y0 (peptide with no glycan) in *O*-glycopeptide spectra.[114] Figure S19 shows the percentage of ETD, EThcD, HCD, and sceHCD spectra that have Y0, Y1, and two different Y2 ions, peptide+HexNAc(2) versus peptide+HexNAc(1)Hex(1). Note that these data do not comment on the abundance of Y-type ions, merely their presence in spectra. As expected, Y1 is seen in the vast majority of HCD and sceHCD *N*-glycopeptide spectra, although higher collision energies (e.g., HCD40) reduce its presence. Y0 is also expected for *N*-glycopeptides, although to a lesser degree,[115] as is observed. Y1 is present in the majority (>80%) of the EThcD25 and EThcD35 *N*-glycopeptide spectra as well, while Y0 is only in ∼35 and 60%, respectively. The pattern of Y0 and Y1 ions effectively flips for *O*-glycopeptides, where Y0 is more often present, especially in EThcD25, EThcD35, and sceHCD spectra. Y1 is less reliably observed in *O*-glycopeptide spectra, although still in relatively high proportions (60−80%) for EThcD25, EThcD35, and sceHCD30 methods. Y2 peptide +HexNAc(2) occurs frequently (>80%) in *N*-glycopeptide spectra in lower to middle HCD energies (20−30 nce) and

https://dx.doi.org/10.1021/acs.jproteome.0c00218
J. Proteome Res. 2020, 19, 3286−3301

sceHCD30 methods, while it is less frequently observed in EThcD and higher energy HCD spectra. This Y2 ion is rarely (<20%) observed in *O*-glycopeptide spectra, as it would be a GalNAc-GlcNAc moiety indicative of core-2 *O*-glycans (which occurs less frequently in the recombinant mucins used in this study). However, higher HCD energies tend to be more favorable for generating it in the *O*-glycopeptide spectra where it should exist. The more common Y2 species for *O*-glycopeptides, peptide+HexNAc(1)Hex(1), is not a possibility for *N*-glycopeptides but represents the common core-1 *O*-glycan structure (GalNAc-Gal). sceHCD methods appear to be the most favorable fragmentation conditions for generating this Y2 ion, although it was also observed in ∼50% of EThcD25 and EThcD35 *O*-glycopeptide spectra. The presence of these Y-type ions can be useful when designing search strategies best suited for dissociation type and glycopeptide class.

Pap et al. recently compared HCD and EThcD for *O*-glycopeptides and observed larger oxonium (B-type) glycan fragments in EThcD spectra.[64] Large oxonium ions can be valuable in confirming glycan composition and determining structural aspects of the sugar. One such ion was the HexNAc(1)Hex(1)NeuAc(1) fragment, 657.2349 *m*/*z*, which can be present in both *N*- and *O*-glycopeptide spectra. We screened spectra that had at least one of the two NeuAc oxonium ions (274.0921 and/or 292.1027 *m*/*z*) for the presence of 657 *m*/*z* (Figure S19). EThcD methods, sceHCD methods except sceHCD35 ± 5, and HCD20-25 all generated the 657 *m*/*z* oxonium ion in at least 80% of Neu5Ac-containing *N*-glycopeptide spectra, with EThcD25 having the highest percentage at ∼96% of spectra. Higher energy HCD activation, however, caused a precipitous loss of the 657 *m*/*z* peak. For *O*-glycopeptides, the 657 *m*/*z* peak was most often observed in sceHCD30 spectra (∼80%), while only 70−75% of EThcD25 and EThcD35 spectra had the fragment. This is slightly lower than that reported by Pap et al., but it highlights that EThcD, sceHCD, and lower energy HCD can generate useful higher mass oxonium ions.

One final observation compared low-mass oxonium ions (Figure S20). Halim et al. showed that the ratio of low-mass oxonium ions can indicate the presence of GalNAc (*O*-glycopeptide) or GlcNAc (*N*-glycopeptides) residues, and oxonium ions have since been used to classify glycopeptide classes and sialylation states.[116−119] We calculated the ratio of 138.055 and 144.0655 *m*/*z* oxonium ions for all scout HCD scans from *N*- and *O*-glycopeptide data sets and plotted their distributions in Figure S20a. *N*- and *O*-glycopeptides have distinct distributions, as predicted, with most *O*-glycopeptides producing a ratio < 3 (median = 1.11) and most *N*-glycopeptides producing a ratio > 5 (median = 16.04). A minor number of higher ratio values for *O*-glycopeptides likely come from species harboring core-2 glycans, which contain a GlcNAc residue. Higher energy HCD and sceHCD triggered scans for *N*-glycopeptides recapitulated ratios from scout HCD scans (Figure S20b), while EThcD35 and lower energy HCD methods slightly overestimated the ratio. Ratios could not be reliably calculated for ETD, EThcD15, or EThcD25 spectra. For *O*-glycopeptides, ratios were detected in EThcD25, although the ratio was slightly underestimated (Figure S20c). Otherwise, EThcD35 and all HCD and sceHCD faithfully reported the 138/144 ratios seen in scout HCD scans. This shows that oxonium ion ratios can be successfully used in sceHCD methods and in some EThcD scans, depending on the method parameters and glycopeptide class.

CONCLUSIONS

Ideally, *N*- and *O*-glycopeptides would share the same optimal dissociation method so that all classes could be analyzed with the same approaches. Here, we compared HCD, sceHCD, ETD, and EThcD methods for mixtures of *N*- and *O*-glycopeptides, determining their identification rates, spectral quality, and suitability for the different glycopeptide classes. Results are summarized in Table 1. Despite the superior spectral quality of EThcD, HCD and sceHCD methods provide more rapid scan acquisition rates to improve identifications and have fragmentation quality sufficient for *N*-glycopeptide identification. Only 60−80% of localized *N*-glycoPSMs from HCD and sceHCD methods in this study had spectral evidence for the localized *N*-glycosite. The vast majority of *N*-glycosites, however, occur in sequences with only one *N*-sequon, making peptide backbone and glycan composition identification acceptable. sceHCD methods provide a slight boost in spectral quality over standard HCD and, thus, are the recommended method for *N*-glycopeptides. sceHCD30 ± 10 generally performed the best in this study, as has been reported elsewhere,[78] yet a recent report argues that a method using stepped collision energies of 20/30/30 may be superior.[86] We saw that sceHCD35 ± 15 also generally performs well, indicating that steps that cover a wide range of energies can be beneficial. On the contrary, HCD and sceHCD are mostly inadequate for site-specific *O*-glycopeptide analysis. Instead, EThcD methods are necessary due to challenges in localizing *O*-glycosites. EThcD25 gave the best localization rates, but EThcD35 provided slightly more *O*-glycoPSMs. Notably, proteolysis with the professional mucinase StcE also improved our ability to characterize *O*-glycopeptides with EThcD.

Our findings have important implications for many choices glycoproteomic researchers must face. First, MS instrument platforms govern access to dissociation methods, and it is crucial to know if desired experiments require access to ETD-enabled systems, such as Orbitrap Tribrid or solariX XR instruments,[99,120−122] or can be successfully completed with HCD-centric systems, e.g., time-of-flight instruments and the Q-Exactive or Exploris platforms.[123,124] Looking forward, ion

Table 1. Summary of Dissociation Method Strengths for *N*- and *O*-Glycopeptides[a]

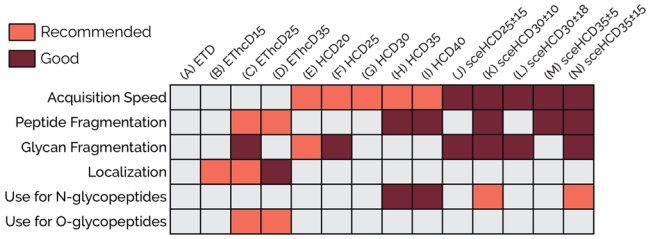

[a]Performances of each HCD-pd-X method tested is considered for four figures of merit, i.e., acquisition speed, quality of peptide backbone fragmentation, quality of glycan fragmentation, and the ability to localize glycosites. HCD and sceHCD methods are recommended for *N*-glycopeptides, and EThcD methods are recommended for *O*-glycopeptides. Although EThcD methods are superior for generating spectral evidence to support *N*-glycosite localization, acquisition speed, balance of peptide and glycan fragmentation, and general presence of only one *N*-glycosite per peptide make sceHCD methods the recommended choice for *N*-glycopeptides.

https://dx.doi.org/10.1021/acs.jproteome.0c00218
J. Proteome Res. 2020, 19, 3286−3301

mobility is gaining traction in many proteomic areas including glycoproteomics,[125,126] and applications like trapped ion mobility spectrometry on the timsTOF system may prove valuable.[127] That said, timsTOF instruments currently rely on collisional dissociation and may not yet be ready for *O*-glycoproteomic applications, while the SNYAPT platforms offer traveling wave ion mobility spectrometry on an ETD-enabled system.[128] A recently described ECD cell may bring electron-driven dissociation to a wider breadth of instrument platforms, too.[129,130]

Dissociation method choice also affects experimental design. sceHCD has been shown to benefit reporter ion generation without detrimental effects on peptide identification in isobaric labeling experiments,[131] yet relatively few studies to date have employed isobaric labeling strategies for glycoproteomic experiments.[44,50,132−136] Perhaps, adoption of sceHCD methods for *N*-glycopeptides will enable more widespread use of isobaric labels, while combinations of HCD and EThcD would still permit isobaric label-based quantitation in *O*-glycoproteomic workflows. Alternatively, the benefits of data-independent acquisition (DIA), which largely relies on collisional dissociation, have been shown for *N*-glycoproteomics.[137−140] That said, there may be caveats for DIA methods for *O*-glycoproteomic applications because of the requirement of ETD-based methods. Indeed, Vakhrushev and co-workers recently reported a DIA method for *O*-glycopeptides, but site-specific analysis came from separate ETD-based acquisitions.[141] This perspective will be critical when mining old data sets for glycopeptide identifications, too, as this approach will likely better suit *N*-glycopeptides than *O*-glycopeptides due to more ubiquitous HCD methods.[142]

In addition to instrumentation and method development, data analysis software is required to interpret glycopeptide spectra, and the choice of dissociation method currently dictates which analysis pipelines are available.[143] A multitude of methods exist for the interpretation of HCD and sceHCD spectra of *N*-glycopeptides,[54,78,81,144−148] but many of these do not have ETD functionalities. Several approaches to interpret HCD and sceHCD spectra of *O*-glycopeptides are emerging,[149−151] but strategies to couple these to concomitant ETD spectral analyses are only beginning to develop.[63] Byonic and Protein Prospector remain the two main pipelines to analyze ETD and EThcD spectra for glycoproteomics. If *O*-glycoproteome analysis is to improve, more software suites that can handle EThcD spectra must emerge, and we must keep improving Byonic and Protein Prospector as the tools we have in hand. We show here that *N*- and *O*-glycopeptides produce fundamentally different spectra, and tools tailored to each are needed. As such, we hope that this dataset provides a useful resource to benchmark new software tools for both *N*- and *O*-glycoproteomic applications.

In closing, this study is the first to comprehensively compare HCD, sceHCD, ETD, and EThcD in head-to-head methods for both *N*- and *O*-glycoproteomic analyses. With these data, we conclude that *N*-glycoproteomics should move forward with sceHCD methods while *O*-glycoproteomics must continue to rely on ETD and EThcD, a fact that is unlikely to change unless novel noncollision-based dissociation methods emerge. This knowledge is not only informative to glycoproteomic methodological choices made today but is also instructional for future considerations in method and software development.

■ ASSOCIATED CONTENT

Supporting Information

The Supporting Information is available free of charge at https://pubs.acs.org/doi/10.1021/acs.jproteome.0c00218.

Figure S1, standard glycoproteins used in this study; Figure S2, testing a range of HCD collision energies; Figure S3, scan counts for the different dissociation methods; Figure S4, localization information for *N*-glycoPSMs; Figure S5, glycosite distance from C-terminus in ETD and EThcD localized NglycoPSMs; Figure S6, *N*-glycoPSMs identified with multiple *N*-glycosites; Figure S7, distributions of fragment ion types for *N*- and *O*-glycopeptides; Figure S8, median values for fragment ion type counts from each method; Figure S9, percent of total ion current explained; Figure S10, fragment signal distribution for *N*-glycopeptides; Figure S11, localized *O*-glycoPSM identifications from standard glycoprotein mix; Figure S12, localization information for *O*-glycoPSMs; Figure S13, fragment signal distribution for *O*-glycopeptides; Figure S14, precursor length and *m*/*z* characterizations for *N*- and *O*-glycoPSMs; Figure S15, precursor ion charge state distributions for *N*-glycoPSMs; Figure S16, precursor ion charge state distributions for *O*-glycoPSMs; Figure S17, distributions of Delta Mod scores for *N*- and *O*-glycoPSMs for different dissociation methods; Figure S18, Byonic does not score the EThcD spectra as well as it scores the HCD spectra; Figure S19, presence of specific Y-type ions in the *N*- and *O*-glycopeptide spectra; and Figure S20, oxonium ion ratios in the *N*- and *O*-glycopeptide spectra (PDF)

Product ion tables exported from Byonic for the annotated spectra in Figures 3 and 7 (XLSX)

■ AUTHOR INFORMATION

Corresponding Author

Carolyn R. Bertozzi − *Department of Chemistry, Stanford University, Stanford, California 94305-6104, United States; Howard Hughes Medical Institute, Stanford, California 94305-6104, United States;* orcid.org/0000-0003-4482-2754; Email: bertozzi@stanfored.edu

Authors

Nicholas M. Riley − *Department of Chemistry, Stanford University, Stanford, California 94305-6104, United States;* orcid.org/0000-0002-1536-2966

Stacy A. Malaker − *Department of Chemistry, Stanford University, Stanford, California 94305-6104, United States;* orcid.org/0000-0003-2382-5067

Marc D. Driessen − *Department of Chemistry, Stanford University, Stanford, California 94305-6104, United States*

Complete contact information is available at: https://pubs.acs.org/10.1021/acs.jproteome.0c00218

Author Contributions

N.M.R. conceived the study, designed experiments, prepared samples, collected LC−MS/MS data, analyzed data, made figures, wrote the original draft, and edited/reviewed the manuscript. S.A.M. and M.D.D. prepared samples and edited/reviewed the manuscript. C.R.B. oversaw all steps of the study and edited/reviewed the manuscript. All authors have given approval to the final version of the manuscript.

https://dx.doi.org/10.1021/acs.jproteome.0c00218
J. Proteome Res. 2020, 19, 3286−3301

Notes

The authors declare the following competing financial interest(s): C.R.B. is a co-founder and Scientific Advisory Board member of Lycia Therapeutics, Palleon Pharmaceuticals, Enable Bioscience, Redwood Biosciences (a subsidiary of Catalent), and InterVenn Biosciences, and a member of the Board of Directors of Eli Lilly and Company.

Raw data files, Byonic output files, filtered glycoPSM files, fasta files, and glycan databases used in this study have been deposited to the ProteomeXchange Consortium via the PRIDE[152] partner repository with the dataset identifier PXD017646 (username: reviewer31453@ebi.ac.uk, password: xUm2JE4z).

■ ACKNOWLEDGMENTS

The authors gratefully acknowledge support from Howard Hughes Medical Institute and National Institute of Health (NIH) Grant R01 CA200423 awarded to C.R.B (need to update this). N.M.R. was funded through an NIH Predoctoral to Postdoctoral Transition Award (Grant K00 CA21245403). S.A.M. was supported by an NIH F32 Postdoctoral Fellowship (F32-GM126663-01). M.D.D. was funded by NIH grant U01-CA207702 (awarded to C.R.B.). The authors also thank Prof. Sharon Pitteri and Abel Bermudez for helpful discussions.

■ REFERENCES

(1) Varki, A.; Cummings, R. D.; Esko, J. D.; Stanley, P.; Hart, G. W.; Aebi, M.; Darvill, A. G.; Kinoshita, T.; Packer, N. H.; Prestegard, J. H.; Schnaar, R. L. Eubacteria. *Essentials of Glycobiology*; Cold Spring Harbor Laboratory Press: 2017.

(2) Moremen, K. W.; Tiemeyer, M.; Nairn, A. V. Vertebrate Protein Glycosylation: Diversity, Synthesis and Function. *Nat. Rev. Mol. Cell Biol.* **2012**, 448−462.

(3) Thaysen-Andersen, M.; Packer, N. H. Advances in LC-MS/MS-Based Glycoproteomics: Getting Closer to System-Wide Site-Specific Mapping of the N- and O-Glycoproteome. *Biochim. Biophys. Acta, Proteins Proteomics* **2014**, 1437−1452.

(4) Leymarie, N.; Griffin, P. J.; Jonscher, K.; Kolarich, D.; Orlando, R.; McComb, M.; Zaia, J.; Aguilan, J.; Alley, W. R.; Altmann, F.; et al. Interlaboratory Study on Differential Analysis of Protein Glycosylation by Mass Spectrometry: The ABRF Glycoprotein Research Multi-Institutional Study 2012. *Mol. Cell. Proteomics* **2013**, *12*, 2935−2951.

(5) Palaniappan, K. K.; Bertozzi, C. R. Chemical Glycoproteomics. *Chem. Rev.* **2016**, *116*, 14277−14306.

(6) Hu, H.; Khatri, K.; Zaia, J. Algorithms and Design Strategies towards Automated Glycoproteomics Analysis. *Mass Spectrom. Rev.* **2017**, 475−498.

(7) Yang, Y.; Franc, V.; Heck, A. J. R. Glycoproteomics: A Balance between High-Throughput and In-Depth Analysis. *Trends Biotechnol.* **2017**, *35*, 598−609.

(8) Ruhaak, L. R.; Xu, G.; Li, Q.; Goonatilleke, E.; Lebrilla, C. B. Mass Spectrometry Approaches to Glycomic and Glycoproteomic Analyses. *Chem. Rev.* **2018**, *118*, 7886−7930.

(9) Xiao, H.; Sun, F.; Suttapitugsakul, S.; Wu, R. Global and Site-specific Analysis of Protein Glycosylation in Complex Biological Systems with Mass Spectrometry. *Mass Spectrom. Rev.* **2019**, *38*, 356−379.

(10) Olsen, J. V.; Macek, B.; Lange, O.; Makarov, A.; Horning, S.; Mann, M. Higher-Energy C-Trap Dissociation for Peptide Modification Analysis. *Nat. Methods* **2007**, *4*, 709−712.

(11) Wuhrer, M.; Catalina, M. I.; Deelder, A. M.; Hokke, C. H. Glycoproteomics Based on Tandem Mass Spectrometry of Glycopeptides. *J. Chromatogr., B: Anal. Technol. Biomed. Life Sci.* **2007**, *849*, 115−128.

(12) Segu, Z. M.; Mechref, Y. Characterizing Protein Glycosylation Sites through Higher-Energy C-Trap Dissociation. *Rapid Commun. Mass Spectrom.* **2010**, *24*, 1217−1225.

(13) Mayampurath, A. M.; Wu, Y.; Segu, Z. M.; Mechref, Y.; Tang, H. Improving Confidence in Detection and Characterization of Protein N-Glycosylation Sites and Microheterogeneity. *Rapid Commun. Mass Spectrom.* **2011**, *25*, 2007−2019.

(14) Syka, J. E. P.; Coon, J. J.; Schroeder, M. J.; Shabanowitz, J.; Hunt, D. F. Peptide and Protein Sequence Analysis by Electron Transfer Dissociation Mass Spectrometry. *Proc. Natl. Acad. Sci. U. S. A.* **2004**, *101*, 9528−9533.

(15) Riley, N. M.; Coon, J. J. The Role of Electron Transfer Dissociation in Modern Proteomics. *Anal. Chem.* **2018**, *90*, 40−64.

(16) Håkansson, K.; Cooper, H. J.; Emmett, M. R.; Costello, C. E.; Marshall, A. G.; Nilsson, C. L. Electron Capture Dissociation and Infrared Multiphoton Dissociation MS/MS of an N-Glycosylated Tryptic Peptide to Yield Complementary Sequence Information. *Anal. Chem.* **2001**, *73*, 4530−4536.

(17) Adamson, J. T.; Håkansson, K. Infrared Multiphoton Dissociation and Electron Capture Dissociation of High-Mannose Type Glycopeptides. *J. Proteome Res.* **2006**, *5*, 493−501.

(18) Hogan, J. M.; Pitteri, S. J.; Chrisman, P. A.; McLuckey, S. A. Complementary Structural Information from a Tryptic N-Linked Glycopeptide via Electron Transfer Ion/Ion Reactions and Collision-Induced Dissociation. *J. Proteome Res.* **2005**, *4*, 628−632.

(19) Alley, W. R., Jr.; Mechref, Y.; Novotny, M. V. Characterization of Glycopeptides by Combining Collision-Induced Dissociation and Electron-Transfer Dissociation Mass Spectrometry Data. *Rapid Commun. Mass Spectrom.* **2009**, *23*, 161−170.

(20) Mechref, Y. Use of CID/ETD Mass Spectrometry to Analyze Glycopeptides. *Curr. Protoc. Protein Sci.* **2012**, *68*, 12−11.

(21) Scott, N. E.; Parker, B. L.; Connolly, A. M.; Paulech, J.; Edwards, A. V. G.; Crossett, B.; Falconer, L.; Kolarich, D.; Djordjevic, S. P.; Højrup, P.; et al. Simultaneous Glycan-Peptide Characterization Using Hydrophilic Interaction Chromatography and Parallel Fragmentation by CID, Higher Energy Collisional Dissociation, and Electron Transfer Dissociation MS Applied to the N-Linked Glycoproteome of Campylobacter jejuni. *Mol. Cell. Proteomics* **2011**, *10*, M000031−MCP201.

(22) Parker, B. L.; Thaysen-Andersen, M.; Solis, N.; Scott, N. E.; Larsen, M. R.; Graham, M. E.; Packer, N. H.; Cordwell, S. J. Site-Specific Glycan-Peptide Analysis for Determination of N-Glycoproteome Heterogeneity. *J. Proteome Res.* **2013**, *12*, 5791−5800.

(23) Woo, C. M.; Felix, A.; Byrd, W. E.; Zuegel, D. K.; Ishihara, M.; Azadi, P.; Iavarone, A. T.; Pitteri, S. J.; Bertozzi, C. R. Development of IsoTaG, a Chemical Glycoproteomics Technique for Profiling Intact N- and O-Glycopeptides from Whole Cell Proteomes. *J. Proteome Res.* **2017**, *16*, 1706−1718.

(24) Totten, S. M.; Feasley, C. L.; Bermudez, A.; Pitteri, S. J. Parallel Comparison of N-Linked Glycopeptide Enrichment Techniques Reveals Extensive Glycoproteomic Analysis of Plasma Enabled by SAX-ERLIC. *J. Proteome Res.* **2017**, *16*, 1249−1260.

(25) Medzihradszky, K. F.; Kaasik, K.; Chalkley, R. J. Tissue-Specific Glycosylation at the Glycopeptide Level. *Mol. Cell. Proteomics* **2015**, *14*, 2103−2110.

(26) Trinidad, J. C.; Schoepfer, R.; Burlingame, A. L.; Medzihradszky, K. F. N- and O-Glycosylation in the Murine Synaptosome. *Mol. Cell. Proteomics* **2013**, *12*, 3474−3488.

(27) Stavenhagen, K.; Kayili, H. M.; Holst, S.; Koeleman, C. A. M.; Engel, R.; Wouters, D.; Zeerleder, S.; Salih, B.; Wuhrer, M. N- and O-Glycosylation Analysis of Human C1-Inhibitor Reveals Extensive Mucin-Type O-Glycosylation. *Mol. Cell. Proteomics* **2018**, *17*, 1225−1238.

(28) Stavenhagen, K.; Gahoual, R.; Dominguez Vega, E.; Palmese, A.; Ederveen, A. L. H.; Cutillo, F.; Palinsky, W.; Bierau, H.; Wuhrer, M. Site-Specific N- and O-Glycosylation Analysis of Atacicept. *mAbs* **2019**, *11*, 1053−1063.

(29) Liu, G.; Cheng, K.; Lo, C. Y.; Li, J.; Qu, J.; Neelamegham, S. A Comprehensive, Open-Source Platform for Mass Spectrometry-Based Glycoproteomics Data Analysis. *Mol. Cell. Proteomics* **2017**, *16*, 2032−2047.

https://dx.doi.org/10.1021/acs.jproteome.0c00218
J. Proteome Res. 2020, 19, 3286−3301

(30) Singh, C.; Zampronio, C. G.; Creese, A. J.; Cooper, H. J. Higher Energy Collision Dissociation (HCD) Product Ion-Triggered Electron Transfer Dissociation (ETD) Mass Spectrometry for the Analysis of N-Linked Glycoproteins. *J. Proteome Res.* **2012**, *11*, 4517−4525.
(31) Wu, S.-W.; Pu, T.-H.; Viner, R.; Khoo, K.-H. Novel LC-MS^2 Product Dependent Parallel Data Acquisition Function and Data Analysis Workflow for Sequencing and Identification of Intact Glycopeptides. *Anal. Chem.* **2014**, *86*, 5478−5486.
(32) Saba, J.; Dutta, S.; Hemenway, E.; Viner, R. Increasing the Productivity of Glycopeptides Analysis by Using Higher-Energy Collision Dissociation-Accurate Mass-Product-Dependent Electron Transfer Dissociation. *Int. J. Proteomics* **2012**, *2012*, 1.
(33) Frese, C. K.; Altelaar, A. F. M.; van den Toorn, H.; Nolting, D.; Griep-Raming, J.; Heck, A. J. R.; Mohammed, S. Toward Full Peptide Sequence Coverage by Dual Fragmentation Combining Electron-Transfer and Higher-Energy Collision Dissociation Tandem Mass Spectrometry. *Anal. Chem.* **2012**, *84*, 9668−9673.
(34) Yu, Q.; Wang, B.; Chen, Z.; Urabe, G.; Glover, M. S.; Shi, X.; Guo, L.-W.; Kent, K. C.; Li, L. Electron-Transfer/Higher-Energy Collision Dissociation (EThcD)-Enabled Intact Glycopeptide/Glycoproteome Characterization. *J. Am. Soc. Mass Spectrom.* **2017**, *28*, 1751−1764.
(35) Glover, M. S.; Yu, Q.; Chen, Z.; Shi, X.; Kent, K. C.; Li, L. Characterization of Intact Sialylated Glycopeptides and Phosphorylated Glycopeptides from IMAC Enriched Samples by EThcD Fragmentation: Toward Combining Phosphoproteomics and Glycoproteomics. *Int. J. Mass Spectrom.* **2018**, *427*, 35−42.
(36) Cao, Q.; Yu, Q.; Liu, Y.; Chen, Z.; Li, L. Signature-Ion-Triggered Mass Spectrometry Approach Enabled Discovery of N- and O-Linked Glycosylated Neuropeptides in the Crustacean Nervous System. *J. Proteome Res.* **2020**, *19*, 634−643.
(37) Zhu, J.; Chen, Z.; Zhang, J.; An, M.; Wu, J.; Yu, Q.; Skilton, S. J.; Bern, M.; Ilker Sen, K.; Li, L.; et al. Differential Quantitative Determination of Site-Specific Intact N-Glycopeptides in Serum Haptoglobin between Hepatocellular Carcinoma and Cirrhosis Using LC-EThcD-MS/MS. *J. Proteome Res.* **2019**, *18*, 359−371.
(38) Riley, N. M.; Hebert, A. S.; Westphall, M. S.; Coon, J. J. Capturing Site-Specific Heterogeneity with Large-Scale N-Glycoproteome Analysis. *Nat. Commun.* **2019**, *10*, 1311.
(39) Reiding, K. R.; Bondt, A.; Franc, V.; Heck, A. J. R. The Benefits of Hybrid Fragmentation Methods for Glycoproteomics. *TrAC, Trends Anal. Chem.* **2018**, 260−268.
(40) Čaval, T.; Zhu, J.; Tian, W.; Remmelzwaal, S.; Yang, Z.; Clausen, H.; Heck, A. J. R. Targeted Analysis of Lysosomal Directed Proteins and Their Sites of Mannose-6-Phosphate Modification. *Mol. Cell. Proteomics* **2019**, *18*, 16−27.
(41) Franc, V.; Yang, Y.; Heck, A. J. R. Proteoform Profile Mapping of the Human Serum Complement Component C9 Revealing Unexpected New Features of N-, O-, and C-Glycosylation. *Anal. Chem.* **2017**, *89*, 3483−3491.
(42) Lin, Y.-H.; Franc, V.; Heck, A. J. R. Similar Albeit Not the Same: In-Depth Analysis of Proteoforms of Human Serum, Bovine Serum, and Recombinant Human Fetuin. *J. Proteome Res.* **2018**, *17*, 2861−2869.
(43) Lin, Y.-H.; Zhu, J.; Meijer, S.; Franc, V.; Heck, A. J. R. Glycoproteogenomics: A Frequent Gene Polymorphism Affects the Glycosylation Pattern of the Human Serum Fetuin/α-2-HS-Glycoprotein. *Mol. Cell. Proteomics* **2019**, *18*, 1479−1490.
(44) Chen, Z.; Yu, Q.; Hao, L.; Liu, F.; Johnson, J.; Tian, Z.; Kao, W. J.; Xu, W.; Li, L. Site-Specific Characterization and Quantitation of N-Glycopeptides in PKM2 Knockout Breast Cancer Cells Using DiLeu Isobaric Tags Enabled by Electron-Transfer/Higher-Energy Collision Dissociation (EThcD). *Analyst* **2018**, *143*, 2508−2519.
(45) Parker, B. L.; Thaysen-Andersen, M.; Fazakerley, D. J.; Holliday, M.; Packer, N. H.; James, D. E. Terminal Galactosylation and Sialylation Switching on Membrane Glycoproteins upon TNF-Alpha-Induced Insulin Resistance in Adipocytes. *Mol. Cell. Proteomics* **2016**, *15*, 141−153.
(46) Cheng, K.; Chen, R.; Seebun, D.; Ye, M.; Figeys, D.; Zou, H. Large-Scale Characterization of Intact N-Glycopeptides Using an Automated Glycoproteomic Method. *J. Proteomics* **2014**, *110*, 145−154.
(47) Sun, S.; Shah, P.; Eshghi, S. T.; Yang, W.; Trikannad, N.; Yang, S.; Chen, L.; Aiyetan, P.; Höti, N.; Zhang, Z.; et al. Comprehensive Analysis of Protein Glycosylation by Solid-Phase Extraction of N-Linked Glycans and Glycosite-Containing Peptides. *Nat. Biotechnol.* **2016**, *34*, 84−88.
(48) Dang, L.; Shen, J.; Zhao, T.; Zhao, F.; Jia, L.; Zhu, B.; Ma, C.; Chen, D.; Zhao, Y.; Sun, S. Recognition of Bisecting *N* -Glycans on Intact Glycopeptides by Two Characteristic Ions in Tandem Mass Spectra. *Anal. Chem.* **2019**, *91*, 5478−5482.
(49) Li, Q.; Kailemia, M. J.; Merleev, A. A.; Xu, G.; Serie, D.; Danan, L. M.; Haj, F. G.; Maverakis, E.; Lebrilla, C. B. Site-Specific Glycosylation Quantitation of 50 Serum Glycoproteins Enhanced by Predictive Glycopeptidomics for Improved Disease Biomarker Discovery. *Anal. Chem.* **2019**, *91*, 5433−5445.
(50) Shah, P.; Wang, X.; Yang, W.; Eshghi, S. T.; Sun, S.; Hoti, N.; Chen, L.; Yang, S.; Pasay, J.; Rubin, A.; et al. Integrated Proteomic and Glycoproteomic Analyses of Prostate Cancer Cells Reveal Glycoprotein Alteration in Protein Abundance and Glycosylation. *Mol. Cell. Proteomics* **2015**, *14*, 2753−2763.
(51) Yang, W.; Shah, P.; Toghi Eshghi, S.; Yang, S.; Sun, S.; Ao, M.; Rubin, A.; Jackson, J. B.; Zhang, H. Glycoform Analysis of Recombinant and Human Immunodeficiency Virus Envelope Protein Gp120 via Higher Energy Collisional Dissociation and Spectral-Aligning Strategy. *Anal. Chem.* **2014**, *86*, 6959−6967.
(52) Lee, J. Y.; Lee, H. K.; Park, G. W.; Hwang, H.; Jeong, H. K.; Yun, K. N.; Ji, E. S.; Kim, K. H.; Kim, J. S.; Kim, J. W.; et al. Characterization of Site-Specific N-Glycopeptide Isoforms of α-1-Acid Glycoprotein from an Interlaboratory Study Using LC-MS/MS. *J. Proteome Res.* **2016**, *15*, 4146−4164.
(53) Kolarich, D.; Jensen, P. H.; Altmann, F.; Packer, N. H. Determination of Site-Specific Glycan Heterogeneity on Glycoproteins. *Nat. Protoc.* **2012**, *7*, 1285−1298.
(54) Stadlmann, J.; Taubenschmid, J.; Wenzel, D.; Gattinger, A.; Dürnberger, G.; Dusberger, F.; Elling, U.; Mach, L.; Mechtler, K.; Penninger, J. M. Comparative Glycoproteomics of Stem Cells Identifies New Players in Ricin Toxicity. *Nature* **2017**, *549*, 538−542.
(55) Yang, G.; Hu, Y.; Sun, S.; Ouyang, C.; Yang, W.; Wang, Q.; Betenbaugh, M.; Zhang, H. Comprehensive Glycoproteomic Analysis of Chinese Hamster Ovary Cells. *Anal. Chem.* **2018**, *90*, 14294−14302.
(56) Thaysen-Andersen, M.; Packer, N. H.; Schulz, B. L. Maturing Glycoproteomics Technologies Provide Unique Structural Insights into the N-Glycoproteome and Its Regulation in Health and Disease. *Mol. Cell. Proteomics* **2016**, *15*, 1773−1790.
(57) Hevér, H.; Darula, Z.; Medzihradszky, K. F. Characterization of Site-Specific N-Glycosylation. In *Methods in Molecular Biology*; Humana Press: 2019, *1934*, 93−125.
(58) You, X.; Qin, H.; Ye, M. Recent Advances in Methods for the Analysis of Protein O-Glycosylation at Proteome Level. *J. Sep. Sci.* **2018**, 248−261.
(59) Levery, S. B.; Steentoft, C.; Halim, A.; Narimatsu, Y.; Clausen, H.; Vakhrushev, S. Y. Advances in Mass Spectrometry Driven O-Glycoproteomics. *Biochim. Biophys. Acta, Gen. Subj.* **2015**, 33−42.
(60) Darula, Z.; Pap, Á.; Medzihradszky, K. F. Extended Sialylated O-Glycan Repertoire of Human Urinary Glycoproteins Discovered and Characterized Using Electron-Transfer/Higher-Energy Collision Dissociation. *J. Proteome Res.* **2019**, *18*, 280−291.
(61) Darula, Z.; Sarnyai, F.; Medzihradszky, K. F. O-Glycosylation Sites Identified from Mucin Core-1 Type Glycopeptides from Human Serum. *Glycoconjugate J.* **2016**, *33*, 435−445.
(62) Medzihradszky, K. F.; Kaasik, K.; Chalkley, R. J. Characterizing Sialic Acid Variants at the Glycopeptide Level. *Anal. Chem.* **2015**, *87*, 3064−3071.
(63) Zhao, X.; Zheng, S.; Li, Y.; Huang, J.; Zhang, W.; Xie, Y.; Qin, W.; Qian, X. An Integrated Mass Spectroscopy Data Processing Strategy for Fast Identification, In-Depth, and Reproducible Quantification of Protein O-Glycosylation in a Large Cohort of Human Urine Samples. *Anal. Chem.* **2019**, *92*, 690−698.

https://dx.doi.org/10.1021/acs.jproteome.0c00218
J. Proteome Res. 2020, 19, 3286−3301

(64) Pap, A.; Klement, E.; Hunyadi-Gulyas, E.; Darula, Z.; Medzihradszky, K. F. Status Report on the High-Throughput Characterization of Complex Intact O-Glycopeptide Mixtures. *J. Am. Soc. Mass Spectrom.* **2018**, *29*, 1210−1220.
(65) Zhu, Z.; Su, X.; Clark, D. F.; Go, E. P.; Desaire, H. Characterizing O-Linked Glycopeptides by Electron Transfer Dissociation: Fragmentation Rules and Applications in Data Analysis. *Anal. Chem.* **2013**, *85*, 8403−8411.
(66) Khoo, K.-H. Advances toward Mapping the Full Extent of Protein Site-Specific O-GalNAc Glycosylation That Better Reflects Underlying Glycomic Complexity. *Curr. Opin. Struct. Biol.* **2019**, *56*, 146−154.
(67) Darula, Z.; Medzihradszky, K. F. Analysis of Mammalian O-Glycopeptides−We Have Made a Good Start, but There Is a Long Way to Go. *Mol. Cell. Proteomics* **2018**, *17*, 2−17.
(68) Windwarder, M.; Altmann, F. Site-Specific Analysis of the O-Glycosylation of Bovine Fetuin by Electron-Transfer Dissociation Mass Spectrometry. *J. Proteomics* **2014**, *108*, 258−268.
(69) Zhang, Y.; Xie, X.; Zhao, X.; Tian, F.; Lv, J.; Ying, W.; Qian, X. Systems Analysis of Singly and Multiply O-Glycosylated Peptides in the Human Serum Glycoproteome via EThcD and HCD Mass Spectrometry. *J. Proteomics* **2018**, *170*, 14−27.
(70) Malaker, S. A.; Ferracane, M. J.; Depontieu, F. R.; Zarling, A. L.; Shabanowitz, J.; Bai, D. L.; Topalian, S. L.; Engelhard, V. H.; Hunt, D. F. Identification and Characterization of Complex Glycosylated Peptides Presented by the MHC Class II Processing Pathway in Melanoma. *J. Proteome Res.* **2017**, *16*, 228−237.
(71) Marino, F.; Bern, M.; Mommen, G. P. M.; Leney, A. C.; van Gaans-van den Brink, J. A. M.; Bonvin, A. M. J. J.; Becker, C.; van Els, C. A. C. M.; Heck, A. J. R. Extended O-GlcNAc on HLA Class-I-Bound Peptides. *J. Am. Chem. Soc.* **2015**, *137*, 10922−10925.
(72) Yu, Q.; Canales, A.; Glover, M. S.; Das, R.; Shi, X.; Liu, Y.; Keller, M. P.; Attie, A. D.; Li, L. Targeted Mass Spectrometry Approach Enabled Discovery of *O*-Glycosylated Insulin and Related Signaling Peptides in Mouse and Human Pancreatic Islets. *Anal. Chem.* **2017**, *89*, 9184−9191.
(73) Darula, Z.; Chalkley, R. J.; Lynn, A.; Baker, P. R.; Medzihradszky, K. F. Improved Identification of O-Linked Glycopeptides from ETD Data with Optimized Scoring for Different Charge States and Cleavage Specificities. *Amino Acids* **2011**, *41*, 321−328.
(74) Pap, A.; Medzihradszky, K. F.; Darula, Z. Using "Spectral Families" to Assess the Reproducibility of Glycopeptide Enrichment: Human Serum O-Glycosylation Revisited. *Anal. Bioanal. Chem.* **2017**, *409*, 539−550.
(75) Cao, L.; Tolić, N.; Qu, Y.; Meng, D.; Zhao, R.; Zhang, Q.; Moore, R. J.; Zink, E. M.; Lipton, M. S.; Paša-Tolić, L.; et al. Characterization of Intact N- and O-Linked Glycopeptides Using Higher Energy Collisional Dissociation. *Anal. Biochem.* **2014**, *452*, 96−102.
(76) Hinneburg, H.; Stavenhagen, K.; Schweiger-Hufnagel, U.; Pengelley, S.; Jabs, W.; Seeberger, P. H.; Silva, D. V.; Wuhrer, M.; Kolarich, D. The Art of Destruction: Optimizing Collision Energies in Quadrupole-Time of Flight (Q-TOF) Instruments for Glycopeptide-Based Glycoproteomics. *J. Am. Soc. Mass Spectrom.* **2016**, *27*, 507−519.
(77) Yang, H.; Yang, C.; Sun, T. Characterization of Glycopeptides Using a Stepped Higher-Energy C-Trap Dissociation Approach on a Hybrid Quadrupole Orbitrap. *Rapid Commun. Mass Spectrom.* **2018**, *32*, 1353−1362.
(78) Liu, M.-Q.; Zeng, W.-F.; Fang, P.; Cao, W.-Q.; Liu, C.; Yan, G.-Q.; Zhang, Y.; Peng, C.; Wu, J.-Q.; Zhang, X.-J.; et al. PGlyco 2.0 Enables Precision N-Glycoproteomics with Comprehensive Quality Control and One-Step Mass Spectrometry for Intact Glycopeptide Identification. *Nat. Commun.* **2017**, *8*, 438.
(79) Hoffmann, M.; Pioch, M.; Pralow, A.; Hennig, R.; Kottler, R.; Reichl, U.; Rapp, E. The Fine Art of Destruction: A Guide to In-Depth Glycoproteomic Analyses—Exploiting the Diagnostic Potential of Fragment Ions. *Proteomics* **2018**, *18*, 1800282.
(80) Chandler, K. B.; Mehta, N.; Leon, D. R.; Suscovich, T. J.; Alter, G.; Costello, C. E. Multi-Isotype Glycoproteomic Characterization of Serum Antibody Heavy Chains Reveals Isotype- and Subclass-Specific N-Glycosylation Profiles. *Mol. Cell. Proteomics* **2019**, *18*, 686−703.
(81) Bollineni, R. C.; Koehler, C. J.; Gislefoss, R. E.; Anonsen, J. H.; Thiede, B. Large-Scale Intact Glycopeptide Identification by Mascot Database Search. *Sci. Rep.* **2018**, *8*, 2117.
(82) Wang, Y.; Xu, F.; Xiao, K.; Chen, Y.; Tian, Z. Site- and Structure-Specific Characterization of: N -Glycoprotein Markers of MCF-7 Cancer Stem Cells Using Isotopic-Labelling Quantitative N-Glycoproteomics. *Chem. Commun.* **2019**, *55*, 7934−7937.
(83) Zhang, Y.; Mao, Y.; Zhao, W.; Su, T.; Zhong, Y.; Fu, L.; Zhu, J.; Cheng, J.; Yang, H. Glyco-CPLL: An Integrated Method for In-Depth and Comprehensive N-Glycoproteome Profiling of Human Plasma. *J. Proteome Res.* **2020**, *19*, 655−666.
(84) Fang, P.; Xie, J.; Sang, S.; Zhang, L.; Liu, M.; Yang, L.; Xu, Y.; Yan, G.; Yao, J.; Gao, X.; et al. Multilayered N-Glycoproteome Profiling Reveals Highly Heterogeneous and Dysregulated Protein N-Glycosylation Related to Alzheimer's Disease. *Anal. Chem.* **2020**, *92*, 867−874.
(85) Qin, H.; Chen, Y.; Mao, J.; Cheng, K.; Sun, D.; Dong, M.; Wang, L.; Wang, L.; Ye, M. Proteomics Analysis of Site-Specific Glycoforms by a Virtual Multistage Mass Spectrometry Method. *Anal. Chim. Acta* **2019**, *1070*, 60−68.
(86) Wang, Y.; Tian, Z. New Energy Setup Strategy for Intact N-Glycopeptides Characterization Using Higher-Energy Collisional Dissociation. *J. Am. Soc. Mass Spectrom.* **2020**, *31*, 651−657.
(87) You, X.; Qin, H.; Mao, J.; Tian, Y.; Dong, M.; Guo, Z.; Liang, X.; Wang, L.; Jin, Y.; Ye, M. Highly Efficient Identification of O-GalNAc Glycosylation by an Acid-Assisted Glycoform Simplification Approach. *Proteomics* **2018**, *18*, 1800042.
(88) Kelly, M. I.; Dodds, E. D. Parallel Determination of Polypeptide and Oligosaccharide Connectivities by Energy-Resolved Collison-Induced Dissociation of Protonated O-Glycopeptides Derived from Nonspecific Proteolysis. *J. Am. Soc. Mass Spectrom.* **2020**, *31*, 624−632.
(89) Malaker, S. A.; Pedram, K.; Ferracane, M. J.; Bensing, B. A.; Krishnan, V.; Pett, C.; Yu, J.; Woods, E. C.; Kramer, J. R.; Westerlind, U.; et al. The Mucin-Selective Protease StcE Enables Molecular and Functional Analysis of Human Cancer-Associated Mucins. *Proc. Natl. Acad. Sci. U. S. A.* **2019**, *116*, 7278−7287.
(90) HaileMariam, M.; Eguez, R. V.; Singh, H.; Bekele, S.; Ameni, G.; Pieper, R.; Yu, Y. S-Trap, an Ultrafast Sample-Preparation Approach for Shotgun Proteomics. *J. Proteome Res.* **2018**, *17*, 2917−2924.
(91) Čaval, T.; Zhu, J.; Heck, A. J. R. Simply Extending the Mass Range in Electron Transfer Higher Energy Collisional Dissociation Increases Confidence in N-Glycopeptide Identification. *Anal. Chem.* **2019**, *91*, 10401−10406.
(92) Rose, C. M.; Rush, M. J. P.; Riley, N. M.; Merrill, A. E.; Kwiecien, N. W.; Holden, D. D.; Mullen, C.; Westphall, M. S.; Coon, J. J. A Calibration Routine for Efficient ETD in Large-Scale Proteomics. *J. Am. Soc. Mass Spectrom.* **2015**, *26*, 1848−1857.
(93) Bern, M.; Kil, Y. J.; Becker, C. Byonic: Advanced Peptide and Protein Identification Software. *Curr. Protoc. Bioinf.* **2012**, *40*, 20.
(94) Chalkley, R. J.; Baker, P. R. Use of a Glycosylation Site Database to Improve Glycopeptide Identification from Complex Mixtures. *Anal. Bioanal. Chem.* **2017**, *409*, 571−577.
(95) Khatri, K.; Klein, J. A.; Zaia, J. Use of an Informed Search Space Maximizes Confidence of Site-Specific Assignment of Glycoprotein Glycosylation. *Anal. Bioanal. Chem.* **2017**, *409*, 607−618.
(96) Lee, L. Y.; Moh, E. S. X.; Parker, B. L.; Bern, M.; Packer, N. H.; Thaysen-Andersen, M. Toward Automated N-Glycopeptide Identification in Glycoproteomics. *J. Proteome Res.* **2016**, *15*, 3904−3915.
(97) Alagesan, K.; Hinneburg, H.; Seeberger, P. H.; Silva, D. V.; Kolarich, D. Glycan Size and Attachment Site Location Affect Electron Transfer Dissociation (ETD) Fragmentation and Automated Glycopeptide Identification. *Glycoconjugate J.* **2019**, *36*, 487−493.
(98) Stavenhagen, K.; Hinneburg, H.; Thaysen-Andersen, M.; Hartmann, L.; Silva, D. V.; Fuchser, J.; Kaspar, S.; Rapp, E.; Seeberger, P. H.; Kolarich, D. Quantitative Mapping of Glycoprotein Micro-Heterogeneity and Macro-Heterogeneity: An Evaluation of

https://dx.doi.org/10.1021/acs.jproteome.0c00218
J. Proteome Res. 2020, 19, 3286−3301

Mass Spectrometry Signal Strengths Using Synthetic Peptides and Glycopeptides. *J. Mass Spectrom.* **2013**, *48*, 627−639.
(99) Khatri, K.; Pu, Y.; Klein, J. A.; Wei, J.; Costello, C. E.; Lin, C.; Zaia, J. Comparison of Collisional and Electron-Based Dissociation Modes for Middle-Down Analysis of Multiply Glycosylated Peptides. *J. Am. Soc. Mass Spectrom.* **2018**, *29*, 1075−1085.
(100) Steentoft, C.; Vakhrushev, S. Y.; Vester-Christensen, M. B.; Schjoldager, K. T.-B. G.; Kong, Y.; Bennett, E. P.; Mandel, U.; Wandall, H.; Levery, S. B.; Clausen, H. Mining the O-Glycoproteome Using Zinc-Finger Nuclease-Glycoengineered SimpleCell Lines. *Nat. Methods* **2011**, *8*, 977−982.
(101) Steentoft, C.; Vakhrushev, S. Y.; Joshi, H. J.; Kong, Y.; Vester-Christensen, M. B.; Schjoldager, K. T.-B. G.; Lavrsen, K.; Dabelsteen, S.; Pedersen, N. B.; Marcos-Silva, L.; et al. Precision Mapping of the Human O-GalNAc Glycoproteome through SimpleCell Technology. *EMBO J.* **2013**, *32*, 1478−1488.
(102) Vakhrushev, S. Y.; Steentoft, C.; Vester-Christensen, M. B.; Bennett, E. P.; Clausen, H.; Levery, S. B. Enhanced Mass Spectrometric Mapping of the Human GalNAc-Type O-Glycoproteome with Simplecells. *Mol. Cell. Proteomics* **2013**, *12*, 932−944.
(103) Narimatsu, Y.; Joshi, H. J.; Schjoldager, K. T.; Hintze, J.; Halim, A.; Steentoft, C.; Nason, R.; Mandel, U.; Bennett, E. P.; Clausen, H.; et al. Exploring Regulation of Protein O-Glycosylation in Isogenic Human HEK293 Cells by Differential O-Glycoproteomics. *Mol. Cell. Proteomics* **2019**, *18*, 1396−1409.
(104) Goth, C. K.; Halim, A.; Khetarpal, S. A.; Rader, D. J.; Clausen, H.; Schjoldager, K. T.-B. G. A Systematic Study of Modulation of ADAM-Mediated Ectodomain Shedding by Site-Specific O-Glycosylation. *Proc. Natl. Acad. Sci. U. S. A.* **2015**, *112*, 14623−14628.
(105) King, S. L.; Joshi, H. J.; Schjoldager, K. T.; Halim, A.; Madsen, T. D.; Dziegiel, M. H.; Woetmann, A.; Vakhrushev, S. Y.; Wandall, H. H. Characterizing the O-Glycosylation Landscape of Human Plasma, Platelets, and Endothelial Cells. *Blood Adv.* **2017**, *1*, 429−442.
(106) Domagalski, M. J.; Alocci, D.; Almeida, A.; Kolarich, D.; Lisacek, F. PepSweetener: A Web-Based Tool to Support Manual Annotation of Intact Glycopeptide MS Spectra. *PROTEOMICS: Clin. Appl.* **2018**, *12*, 1700069.
(107) Stavenhagen, K.; Hinneburg, H.; Kolarich, D.; Wuhrer, M. Site-Specific N- and O-Glycopeptide Analysis Using an Integrated C18-PGC-LC-ESI-QTOF-MS/MS Approach. In *Methods in Molecular Biology*; Humana Press: 2017, Vol. *1503*, pp 109−119.
(108) Hoffmann, M.; Marx, K.; Reichl, U.; Wuhrer, M.; Rapp, E. Site-Specific O-Glycosylation Analysis of Human Blood Plasma Proteins. *Mol. Cell. Proteomics* **2016**, *15*, 624−641.
(109) Zauner, G.; Hoffmann, M.; Rapp, E.; Koeleman, C. A. M.; Dragan, I.; Deelder, A. M.; Wuhrer, M.; Hensbergen, P. J. Glycoproteomic Analysis of Human Fibrinogen Reveals Novel Regions of O-Glycosylation. *J. Proteome Res.* **2012**, *11*, 5804−5814.
(110) Yang, W.; Ao, M.; Hu, Y.; Li, Q. K.; Zhang, H. Mapping the O-glycoproteome Using Site-specific Extraction of O-linked Glycopeptides (EXoO). *Mol. Syst. Biol.* **2018**, *14*, No. e8486.
(111) Yang, S.; Onigman, P.; Wu, W. W.; Sjogren, J.; Nyhlen, H.; Shen, R.-F.; Cipollo, J. Deciphering Protein O-Glycosylation: Solid-Phase Chemoenzymatic Cleavage and Enrichment. *Anal. Chem.* **2018**, *90*, 8261−8269.
(112) Bern, M.; Cai, Y.; Goldberg, D. Lookup Peaks: A Hybrid of de Novo Sequencing and Database Search for Protein Identification by Tandem Mass Spectrometry. *Anal. Chem.* **2007**, *79*, 1393−1400.
(113) Riley, N. M.; Coon, J. J. Phosphoproteomics in the Age of Rapid and Deep Proteome Profiling. *Anal. Chem.* **2016**, *88*, 74−94.
(114) Chalkley, R. J.; Medzihradszky, K. F.; Darula, Z.; Pap, A.; Baker, P. R. The Effectiveness of Filtering Glycopeptide Peak List Files for Y Ions. *Mol. Omics* **2020**, *16*, 147−155.
(115) Lynn, K.-S.; Chen, C.-C.; Lih, T. M.; Cheng, C.-W.; Su, W.-C.; Chang, C.-H.; Cheng, C.-Y.; Hsu, W.-L.; Chen, Y.-J.; Sung, T.-Y. MAGIC: An Automated N-Linked Glycoprotein Identification Tool Using a Y1-Ion Pattern Matching Algorithm and *in Silico* MS^2 Approach. *Anal. Chem.* **2015**, *87*, 2466−2473.
(116) Halim, A.; Westerlind, U.; Pett, C.; Schorlemer, M.; Rüetschi, U.; Brinkmalm, G.; Sihlbom, C.; Lengqvist, J.; Larson, G.; Nilsson, J. Assignment of Saccharide Identities through Analysis of Oxonium Ion Fragmentation Profiles in LC−MS/MS of Glycopeptides. *J. Proteome Res.* **2014**, *13*, 6024−6032.
(117) Toghi Eshghi, S.; Yang, W.; Hu, Y.; Shah, P.; Sun, S.; Li, X.; Zhang, H. Classification of Tandem Mass Spectra for Identification of N- and O-Linked Glycopeptides. *Sci. Rep.* **2016**, *6*, 37189.
(118) Pett, C.; Nasir, W.; Sihlbom, C.; Olsson, B.-M.; Caixeta, V.; Schorlemer, M.; Zahedi, R. P.; Larson, G.; Nilsson, J.; Westerlind, U. Effective Assignment of A2,3/A2,6-Sialic Acid Isomers by LC-MS/MS-Based Glycoproteomics. *Angew. Chem., Int. Ed.* **2018**, *57*, 9320−9324.
(119) Yu, J.; Schorlemer, M.; Toledo, A. G.; Pett, C.; Sihlbom, C.; Larson, G.; Westerlind, U.; Nilsson, J. Distinctive MS/MS Fragmentation Pathways of Glycopeptide-Generated Oxonium Ions Provide Evidence of the Glycan Structure. *Chem. - Eur. J.* **2016**, *22*, 1114−1124.
(120) Senko, M. W.; Remes, P. M.; Canterbury, J. D.; Mathur, R.; Song, Q.; Eliuk, S. M.; Mullen, C.; Earley, L.; Hardman, M.; Blethrow, J. D.; et al. Novel Parallelized Quadrupole/Linear Ion Trap/Orbitrap Tribrid Mass Spectrometer Improving Proteome Coverage and Peptide Identification Rates. *Anal. Chem.* **2013**, *85*, 11710−11714.
(121) Riley, N. M.; Mullen, C.; Weisbrod, C. R.; Sharma, S.; Senko, M. W.; Zabrouskov, V.; Westphall, M. S.; Syka, J. E. P.; Coon, J. J. Enhanced Dissociation of Intact Proteins with High Capacity Electron Transfer Dissociation. *J. Am. Soc. Mass Spectrom.* **2016**, *27*, 520−531.
(122) Huguet, R.; Mullen, C.; Srzentić, K.; Greer, J. B.; Fellers, R. T.; Zabrouskov, V.; Syka, J. E. P.; Kelleher, N. L.; Fornelli, L. Proton Transfer Charge Reduction Enables High-Throughput Top-Down Analysis of Large Proteoforms. *Anal. Chem.* **2019**, *91*, 15732−15739.
(123) Kelstrup, C. D.; Bekker-Jensen, D. B.; Arrey, T. N.; Hogrebe, A.; Harder, A.; Olsen, J. V. Performance Evaluation of the Q Exactive HF-X for Shotgun Proteomics. *J. Proteome Res.* **2018**, *17*, 727−738.
(124) Bekker-Jensen, D. B.; Martínez-Val, A.; Steigerwald, S.; Rüther, P.; Fort, K. L.; Arrey, T. N.; Harder, A.; Makarov, A.; Olsen, J. V. A Compact Quadrupole-Orbitrap Mass Spectrometer with FAIMS Interface Improves Proteome Coverage in Short LC Gradients. *Mol. Cell. Proteomics* **2020**, 716.
(125) Zhu, F.; Trinidad, J. C.; Clemmer, D. E. Glycopeptide Site Heterogeneity and Structural Diversity Determined by Combined Lectin Affinity Chromatography/IMS/CID/MS Techniques. *J. Am. Soc. Mass Spectrom.* **2015**, *26*, 1092−1102.
(126) Mookherjee, A.; Guttman, M. Bridging the Structural Gap of Glycoproteomics with Ion Mobility Spectrometry. *Curr. Opin. Chem. Biol.* **2018**, *42*, 86−92.
(127) Meier, F.; Beck, S.; Grassl, N.; Lubeck, M.; Park, M. A.; Raether, O.; Mann, M. Parallel Accumulation−Serial Fragmentation (PASEF): Multiplying Sequencing Speed and Sensitivity by Synchronized Scans in a Trapped Ion Mobility Device. *J. Proteome Res.* **2015**, *14*, 5378−5387.
(128) Fenn, L. S.; McLean, J. A. Simultaneous Glycoproteomics on the Basis of Structure Using Ion Mobility-Mass Spectrometry. *Mol. BioSyst.* **2009**, *5*, 1298−1302.
(129) Shaw, J. B.; Malhan, N.; Vasil'Ev, Y. V.; Lopez, N. I.; Makarov, A.; Beckman, J. S.; Voinov, V. G. Sequencing Grade Tandem Mass Spectrometry for Top-Down Proteomics Using Hybrid Electron Capture Dissociation Methods in a Benchtop Orbitrap Mass Spectrometer. *Anal. Chem.* **2018**, *90*, 10819−10827.
(130) Fort, K. L.; Cramer, C. N.; Voinov, V. G.; Vasil'Ev, Y. V.; Lopez, N. I.; Beckman, J. S.; Heck, A. J. R. Exploring ECD on a Benchtop Q Exactive Orbitrap Mass Spectrometer. *J. Proteome Res.* **2018**, *17*, 926−933.
(131) Diedrich, J. K.; Pinto, A. F. M.; Yates, J. R., III Energy Dependence of HCD on Peptide Fragmentation: Stepped Collisional Energy Finds the Sweet Spot. *J. Am. Soc. Mass Spectrom.* **2013**, *24*, 1690−1699.
(132) Stadlmann, J.; Hoi, D. M.; Taubenschmid, J.; Mechtler, K.; Penninger, J. M. Analysis of PNGase F-Resistant N-Glycopeptides

https://dx.doi.org/10.1021/acs.jproteome.0c00218
J. Proteome Res. 2020, 19, 3286−3301

Using SugarQb for Proteome Discoverer 2.1 Reveals Cryptic Substrate Specificities. *Proteomics* **2018**, *18*, 1700436.
(133) Cho, K.-C.; Chen, L.; Hu, Y.; Schnaubelt, M.; Zhang, H. Developing Workflow for Simultaneous Analyses of Phosphopeptides and Glycopeptides. *ACS Chem. Biol.* **2019**, *14*, 58−66.
(134) Yang, W.; Shah, P.; Hu, Y.; Toghi Eshghi, S.; Sun, S.; Liu, Y.; Zhang, H. Comparison of Enrichment Methods for Intact N- and O-Linked Glycopeptides Using Strong Anion Exchange and Hydrophilic Interaction Liquid Chromatography. *Anal. Chem.* **2017**, *89*, 11193−11197.
(135) Ye, H.; Boyne, M. T., II; Buhse, L. F.; Hill, J. Direct Approach for Qualitative and Quantitative Characterization of Glycoproteins Using Tandem Mass Tags and an LTQ Orbitrap XL Electron Transfer Dissociation Hybrid Mass Spectrometer. *Anal. Chem.* **2013**, *85*, 1531−1539.
(136) Lee, H.-J.; Cha, H.-J.; Lim, J.-S.; Lee, S. H.; Song, S. Y.; Kim, H.; Hancock, W. S.; Yoo, J. S.; Paik, Y.-K. Abundance-Ratio-Based Semiquantitative Analysis of Site-Specific N-Linked Glycopeptides Present in the Plasma of Hepatocellular Carcinoma Patients. *J. Proteome Res.* **2014**, *13*, 2328−2338.
(137) Pan, K.-T.; Chen, C.-C.; Urlaub, H.; Khoo, K.-H. Adapting Data-Independent Acquisition for Mass Spectrometry-Based Protein Site-Specific N-Glycosylation Analysis. *Anal. Chem.* **2017**, *89*, 4532−4539.
(138) Zacchi, L. F.; Schulz, B. L. SWATH-MS Glycoproteomics Reveals Consequences of Defects in the Glycosylation Machinery. *Mol. Cell. Proteomics* **2016**, *15*, 2435−2447.
(139) Zacchi, L. F.; Schulz, B. L. Data-Independent Acquisition for Yeast Glycoproteomics. In *Methods in Molecular Biology*; Humana Press: 2019, Vol. *2049*, pp 191−202.
(140) Zhou, C.; Schulz, B. L. Glycopeptide Variable Window SWATH for Improved Data Independent Acquisition Glycoprotein analysis. *Anal. Biochem.* **2020**, 113667.
(141) Ye, Z.; Mao, Y.; Clausen, H.; Vakhrushev, S. Y. Glyco-DIA: A Method for Quantitative O-Glycoproteomics with in Silico-Boosted Glycopeptide Libraries. *Nat. Methods* **2019**, *16*, 902−910.
(142) Hu, Y.; Shah, P.; Clark, D. J.; Ao, M.; Zhang, H. Reanalysis of Global Proteomic and Phosphoproteomic Data Identified a Large Number of Glycopeptides. *Anal. Chem.* **2018**, *90*, 8065−8071.
(143) Hu, H.; Khatri, K.; Klein, J.; Leymarie, N.; Zaia, J. A Review of Methods for Interpretation of Glycopeptide Tandem Mass Spectral Data. *Glycoconjugate J.* **2016**, *33*, 285−296.
(144) Xiao, K.; Tian, Z. GPSeeker Enables Quantitative Structural N-Glycoproteomics for Site- and Structure-Specific Characterization of Differentially Expressed N-Glycosylation in Hepatocellular Carcinoma. *J. Proteome Res.* **2019**, *18*, 2885−2895.
(145) Pioch, M.; Hoffmann, M.; Pralow, A.; Reichl, U.; Rapp, E. Gly Xtool^{MS}: An Open-Source Pipeline for Semiautomated Analysis of Glycopeptide Mass Spectrometry Data. *Anal. Chem.* **2018**, *90*, 11908−11916.
(146) Toghi Eshghi, S.; Shah, P.; Yang, W.; Li, X.; Zhang, H. GPQuest: A Spectral Library Matching Algorithm for Site-Specific Assignment of Tandem Mass Spectra to Intact n-Glycopeptides. *Anal. Chem.* **2015**, *87*, 5181−5188.
(147) Nasir, W.; Toledo, A. G.; Noborn, F.; Nilsson, J.; Wang, M.; Bandeira, N.; Larson, G. SweetNET: A Bioinformatics Workflow for Glycopeptide MS/MS Spectral Analysis. *J. Proteome Res.* **2016**, *15*, 2826−2840.
(148) Park, G. W.; Kim, J. Y.; Hwang, H.; Lee, J. Y.; Ahn, Y. H.; Lee, H. K.; Ji, E. S.; Kim, K. H.; Jeong, H. K.; Yun, K. N.; et al. Integrated GlycoProteome Analyzer (I-GPA) for Automated Identification and Quantitation of Site-Specific N-Glycosylation. *Sci. Rep.* **2016**, *6*, 21175.
(149) Qin, H.; Cheng, K.; Zhu, J.; Mao, J.; Wang, F.; Dong, M.; Chen, R.; Guo, Z.; Liang, X.; Ye, M.; et al. Proteomics Analysis of O-GalNAc Glycosylation in Human Serum by an Integrated Strategy. *Anal. Chem.* **2017**, *89*, 1469−1476.
(150) Mao, J.; You, X.; Qin, H.; Wang, C.; Wang, L.; Ye, M. A New Searching Strategy for the Identification of O-Linked Glycopeptides. *Anal. Chem.* **2019**, *91*, 3852−3859.
(151) Swearingen, K. E.; Eng, J. K.; Shteynberg, D.; Vigdorovich, V.; Springer, T. A.; Mendoza, L.; Sather, D. N.; Deutsch, E. W.; Kappe, S. H. I.; Moritz, R. L. A Tandem Mass Spectrometry Sequence Database Search Method for Identification of O-Fucosylated Proteins by Mass Spectrometry. *J. Proteome Res.* **2019**, *18*, 652−663.
(152) Perez-Riverol, Y.; Csordas, A.; Bai, J.; Bernal-Llinares, M.; Hewapathirana, S.; Kundu, D. J.; Inuganti, A.; Griss, J.; Mayer, G.; Eisenacher, M.; et al. The PRIDE Database and Related Tools and Resources in 2019: Improving Support for Quantification Data. *Nucleic Acids Res.* **2019**, *47*, D442−D450.

https://dx.doi.org/10.1021/acs.jproteome.0c00218
J. Proteome Res. 2020, 19, 3286−3301